



**BSc Report**

# Boundary Layer over a Flat Plate

P.P. Puttkammer

FACULTY OF ENGINEERING TECHNOLOGY  
Engineering Fluid Dynamics

Examination Committee:

prof. dr. ir. H.W.M Hoeijmakers  
dr. ir. W.K. den Otter  
dr.ir. R. Hagmeijer

Engineering Fluid Dynamics  
Multi Scale Mechanics  
Engineering Fluid Dynamics

Enschede, June 2013

**UNIVERSITY OF TWENTE.**



## Summary

Air flowing past a solid surface will stick to that surface. This phenomenon - caused by viscosity - is a description of the no-slip condition. This condition states that the velocity of the fluid at the solid surface equals the velocity of that surface. The result of this condition is that a boundary layer is formed in which the relative velocity varies from zero at the wall to the value of the relative velocity at some distance from the wall.

The goal of the present research is to measure the velocity profile in the thin boundary layer of a flat plate at zero angle of attack at Reynolds numbers up to 140,000, installed in the Silent Wind Tunnel at the University of Twente. The measured velocity profiles are compared with results from theory.

In the present study this boundary layer is investigated analytically, numerically and experimentally.

First, the boundary-layer equations are derived. This derivation and the assumptions required in the derivation are discussed in some detail.

Second, the boundary-layer equations are solved analytically and numerically for the case of laminar flow. The analytical similarity solution of Blasius is presented. Then approximation methods are carried out and a numerical approach is investigated. These calculations showed that the numerical approach yields velocity profiles that are very similar to Blasius' solution.

Third, velocity measurements have been carried. Hot Wire Anemometry is used to measure the velocity profile inside the boundary layer along the flat plate. A flap at the trailing edge of the flat plate is used to ensure that leading edge of the plate is at zero degree angle of attack. From the experiments it is concluded that the measured velocity profiles fit Blasius' solution. Therefore Hot Wire Anemometry can be used for measuring the velocity distribution within the boundary layer.



# Contents

<b>SUMMARY</b>	<b>III</b>
<b>LIST OF SYMBOLS</b>	<b>VII</b>
<b>1. INTRODUCTION</b>	<b>- 1 -</b>
<b>2 BOUNDARY LAYER</b>	<b>- 3 -</b>
<b>2.1 PRANDTL'S BOUNDARY LAYER</b>	<b>- 3 -</b>
<b>2.2 LAWS OF CONSERVATION</b>	<b>- 3 -</b>
2.2.1 CONTINUITY EQUATION	- 3 -
2.2.2 NAVIER-STOKES EQUATION	- 4 -
<b>2.3 BOUNDARY-LAYER THEORY</b>	<b>- 5 -</b>
<b>3 DERIVATION OF SOLUTION BOUNDARY-LAYER EQUATIONS</b>	<b>- 9 -</b>
<b>3.1 ANALYTICAL SOLUTIONS</b>	<b>- 9 -</b>
3.1.1 BLASIUS' EQUATION	- 9 -
3.1.2 SHOOTING METHOD	- 11 -
3.1.3 RESULTS	- 12 -
<b>3.2 APPROXIMATION SOLUTIONS</b>	<b>- 17 -</b>
3.2.1 MOMENTUM-INTEGRAL EQUATION	- 17 -
3.2.2 APPROXIMATION VELOCITY PROFILE	- 18 -
3.2.3 RESULTS	- 20 -
<b>3.3 NUMERICAL SOLUTIONS</b>	<b>- 23 -</b>
3.3.1 EXPLICIT DISCRETISATION	- 23 -
3.3.2 STEP SIZE	- 24 -
3.3.2 RESULTS	- 24 -
<b>3.4 CONCLUSIONS</b>	<b>- 26 -</b>
3.4.1 VELOCITY PROFILE	- 26 -
3.4.2 SKIN FRICTION COEFFICIENT	- 27 -
3.4.3 BOUNDARY LAYER THICKNESS	- 28 -
<b>4 EXPERIMENTS</b>	<b>- 29 -</b>
<b>4.1 SET-UP</b>	<b>- 29 -</b>
4.1.1 FLOW SPEED MEASUREMENTS IN BOUNDARY LAYER: HOT WIRE ANEMOMETRY	- 29 -
4.1.2 CALIBRATION OF THE HOT WIRE	- 30 -
4.1.3 FLAP	- 30 -
<b>4.2 RESULTS</b>	<b>- 31 -</b>
4.2.1 WITHOUT FLAP	- 31 -
4.2.2 WITH FLAP	- 33 -
<b>4.3 COMPARISON OF DATA</b>	<b>- 33 -</b>
4.3.1 COMPARISON DATA WITH AND WITHOUT FLAP	- 33 -
4.3.2 COMPARISON EXPERIMENTAL DATA WITH THEORY	- 34 -

<b>4.3 DISCUSSION</b>	<b>- 35 -</b>
<b>4.4 CONCLUSIONS</b>	<b>- 36 -</b>
<b>5 CONCLUSIONS AND RECOMMENDATIONS</b>	<b>- 39 -</b>
<b>5.1 MAIN CONCLUSIONS</b>	<b>- 39 -</b>
<b>5.2 RECOMMENDATIONS</b>	<b>- 39 -</b>
<b>6 REFERENCES</b>	<b>- 41 -</b>

---

## List of symbols

$c$	m	length of flat plate	$Re_x$	–	Reynolds number
$c_f$	–	Local skin friction coefficient	$S$	$m^2$	Surface
$C_f$	–	Skin friction coefficient	$t$	s	Time
$C_u$	–	Correction factor for HWA close to the wall	$t_i$	Pa	Stress Vector
$F_i$	N	Force vector	$u$	m/s	Horizontal velocity
$g$	$m/s^2$	Gravitational acceleration	$u_e$	m/s	Horizontal velocity on edge of boundary layer
$l_c$	m	Viscous length	$u_j$	m/s	Velocity vector
$m$	kg	Mass	$u_\tau$	m/s	Friction velocity
$M$	Ns	Momentum	$U_\infty$	m/s	Free stream velocity
$n_j$	–	Normal vector	$v$	m/s	Vertical velocity
$p$	Pa	Pressure	$V$	$m^3$	Volume
$P_e$	Pa	Pressure on edge of boundary layer	$x$	m	Position
$Re_c$	–	Reynolds number at the end of the plate	$y^+$	–	Scaled length
$\Delta x$	m	Displacement in x-direction	$\mu$	Pa s	Dynamic viscosity
$\Delta y$	m	Displacement in y-direction	$\nu$	$m^2/s$	Kinematic viscosity
$\delta$	m	Boundary layer thickness	$\rho$	$kg/m^3$	Density
$\delta^*$	m	Displacement thickness	$\sigma_{ij}$	Pa	Stress tensor
$\theta$	m	Momentum thickness	$\tau$	Pa	Shear stress
$\eta$	–	Dimensionless parameter			



# 1. Introduction

Since the physical description of the boundary layer by Ludwig Prandtl in 1904, there have been many developments in this field. There are improved analytical relations for certain situations and mathematical models, for example implemented in computational methods. However, there is not as much research done on the manipulation of the boundary layer since the 'discovery' of the boundary layer. This can be of interest for studies on efficiency or drag of wings of aircrafts or blades of wind turbines.

The problem addressed in the present research is to carry out experiments on boundary layers. Such experiments are needed to verify the positive effect that is inflicted by techniques to manipulate the boundary layer. In practise, it is still difficult to measure the velocity profiles within the boundary layer. The present study will compare results from the theory of boundary layers with the results from experiments in the most simple setting; a flat plate at zero degrees of incidence at modest Reynolds numbers. In the wind tunnel of the University of Twente measurements have been carried out on the velocity profile within the boundary layer. These measurements will be compared with the relations from theory to assess the accuracy at the measurements.

In short, the goal of this study is to measure the velocity profile in the boundary layer of the flat plate and compare the results with the results from theory.



## 2 Boundary Layer

### 2.1 Prandtl's boundary layer [1]

Early in the 20<sup>th</sup> century the theory of the mechanics of fluids in motion had two seemingly compelling fields of study. On one hand there was hydrodynamics – the theory that described the flow over surfaces and bodies assuming the flow to be inviscid, incompressible and irrotational – and on the other hand there was the field of hydraulics which was a mainly experimental field concerning the behaviour of fluids in machinery like pipes, pumps and ships. Hydrodynamics appeared to be a good theory for flows in the region not close to solid boundaries; however it could not explain concepts like friction and drag. Hydraulics did not provide a solid base to design their experiments since there was too little theory. Ludwig Prandtl provided a theory to connect these fields. He presented his boundary layer theory in 1904 at the third Congress of Mathematicians in Heidelberg, Germany. A boundary layer is the thin region of flow adjacent to a surface, the layer in which the flow is influenced by the friction between the solid surface and the fluid [2]. The theory was based on some important observations. The viscosity of the fluid in motion cannot be neglected in all regions. This leads to a significant condition, the no-slip condition. Flow at the surface of the body is at rest relative to that body. At a certain distance from the body, the viscosity of the flow can again be neglected. This very thin layer close to the body in which the effects of viscosity are important is called the boundary layer. This can also be seen as the layer of fluid in which the tangential component of the velocity of the fluid relative to the body increases from zero at the surface to the free stream value at some distance from the surface.

### 2.2 Laws of conservation

While nobody will question the genius of Prandtl, he did not write down his boundary layer theory after he saw the boundary layer on an apple falling from a tree. Prandtl started with two important physical principles; the conservation of mass and that of momentum. First we will derive the continuity equation and after that the Navier-Stokes equation.

#### 2.2.1 Continuity Equation

The continuity equation describes the conservation of mass. We will start with the definition of the mass  $m$  within a control volume  $V$ :

$$m(t) = \int_{V(t)} \rho(\vec{x}, t) dV \quad (2.1)$$

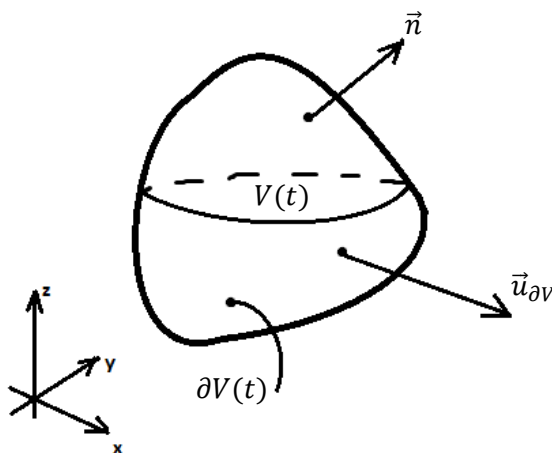


Figure 2.1 Schematic view of control volume

Then the conservation of mass leads to the equation that the time-rate of change of the mass inside  $V(t)$  plus the flux of the mass out of  $V(t)$  through  $\partial V$  should be:

$$\frac{d}{dt} \int_{V(t)} \rho dV + \int_{\partial V} \rho(\vec{u} - \vec{u}_{\partial V}) \vec{n} dS = 0 \quad (2.2)$$

Using the Leibniz-Reynolds transport theorem, since the control volume  $V(t)$  is moving in 3D space:

$$\frac{d}{dt} \int_{V(t)} \rho dV = \int_{V(t)} \frac{\partial \rho}{\partial t} dV + \int_{\partial V(t)} \rho \vec{u}_{\partial V} \vec{n} dS \quad (2.3)$$

And with the notion of the conservation of mass:

$$\int_{V(t)} \frac{\partial \rho}{\partial t} dV + \int_{\partial V(t)} \rho \vec{u} \vec{n} dS = 0 \quad (2.4)$$

Now we want to transform this equation from the integral conservation form to the partial differential form. For this we use Gauss' divergence theorem which states:

$$\int_{V(t)} \vec{\nabla} \cdot \vec{u} dV = \int_{\partial V(t)} \vec{u} \vec{n} dS \quad (2.5)$$

When we substitute this in equation (2.4), the equation will become:

$$\int_{V(t)} \frac{\partial \rho}{\partial t} dV + \int_{V(t)} \vec{\nabla} \cdot (\rho \vec{u}) dV = \int_{V(t)} \left( \frac{\partial \rho}{\partial t} + \vec{\nabla} \cdot (\rho \vec{u}) \right) dV = 0 \quad (2.6)$$

This means that, because  $V(t)$  is an arbitrary control volume, the integrand needs to be zero everywhere, and then the integral conservation equation is transformed into a differential equation; the continuity equation:

$$\boxed{\frac{\partial \rho}{\partial t} + \vec{\nabla} \cdot (\rho \vec{u}) = 0, \quad \text{for } \forall \vec{x} \in V} \quad (2.7)$$

### 2.2.2 Navier-Stokes Equation

The continuity equation describes the conservation of mass in differential form. Similarly, the Navier-Stokes equation describes the conservation of momentum. Here we will start with Newton's second law (with the assumption of mass conservation):

$$m \frac{\partial v_i}{\partial t} = \frac{\partial}{\partial t} (m v_i) = F_i(t) \quad (2.8)$$

This states that the change of momentum of a volume  $\left( \frac{\partial}{\partial t} (m v_i) \right)$  is equal to the force acting on that volume. First we specify the change in momentum:

$$\frac{\partial}{\partial t} \int_{V(t)} \rho \vec{u} dV + \int_{\partial V} \rho \vec{u} ((\vec{u} - \vec{u}_{\partial V}) \vec{n} dS \quad (2.9)$$

Second we will specify the force. There are two contributions to the force on the volume, the force  $\vec{F}_S$  acting on the bounding surface of  $V(t)$  and force  $\vec{F}_v$  acting at each point within the volume.

$$\vec{F}_s = \int_{\partial V(t)} \vec{t} dS = \int_{\partial V(t)} \vec{\sigma} \vec{n} dS \quad (2.10)$$

$$\vec{F}_v = \int_{V(t)} \rho \vec{f} dV \quad (2.11)$$

So the integral conservation equation of momentum is:

$$\frac{\partial}{\partial t} \int_{V(t)} \rho \vec{u} dV + \int_{\partial V} \rho \vec{u} (\vec{u} - \vec{u}_{\partial V}) \vec{n} dS = \int_{\partial V(t)} \vec{\sigma} \vec{n} dS + \int_{V(t)} \rho \vec{f} dV \quad (2.12)$$

Again using the Leibniz-Reynolds transport theorem:

$$\frac{\partial}{\partial t} \int_{V(t)} \rho \vec{u} dV = \int_{V(t)} \frac{\partial}{\partial t} \rho \vec{u} dV + \int_{\partial V(t)} \rho \vec{u} \vec{u}_{\partial V} \vec{n} dS \quad (2.13)$$

Substituting this equation in equation (2.12), we obtain the conservation of momentum in integral form:

$$\int_{V(t)} \frac{\partial}{\partial t} \rho \vec{u} dV + \int_{\partial V(t)} \rho \vec{u} (\vec{u} \vec{n}) dS = \int_{\partial V(t)} \vec{\sigma} \vec{n} dS + \int_{V(t)} \rho \vec{f} dV \quad (2.14)$$

Again with Gauss' theorem (equation (2.5)) we transform the surface integrals into volume integrals, obtaining for arbitrary  $V$  the differential form of the conservation of energy, also known as the Navier-Stokes equation:

$$\boxed{\frac{\partial}{\partial t} \rho \vec{u} + \vec{\nabla}(\rho \vec{u} \vec{u}) = \vec{\nabla}(\vec{\sigma}) + \rho \vec{f}, \quad \text{for } \forall \vec{x} \in V} \quad (2.15)$$

### 2.3 Boundary-layer Theory [2]

We have described the continuity and Navier-Stokes equations. These are the starting point of Prandtl's boundary-layer theory. We will describe steady, incompressible flow. Steady means that the flow at a particular position in space will not change in time. In other words, when taking a picture of for example the flow field around a car (imagine the flow would be visible), the picture will look the same at time  $t$  and time  $t + \Delta t$ , for arbitrary  $\Delta t$ . Incompressible flow means it is not possible to change the density of air. Also we assume to have a 2-dimensional flow within the (x,y) plane. And the last assumption is neglecting the effect of gravity, which will have little influence on the flow inside the boundary layer.

Steady flow	$\frac{\partial \dots}{\partial t} = 0$	two dimensional	$i = 1,2 \ \& \ j = 1,2$
incompressible flow	$\rho = \text{constant}$	no gravity	$\vec{g} = \vec{0}$

These assumptions will change both the continuity equation as well as the Navier-Stokes equations. The continuity equation becomes:

$$\frac{\partial \rho}{\partial t} + \vec{\nabla}(\rho \vec{u}) = \vec{\nabla}(\vec{u}) = 0 \quad (2.16)$$

The Navier-Stokes equations become upon taking  $\rho$  out of the differentials and setting  $g$  to zero:

$$\rho \vec{\nabla}(\vec{u}\vec{u}) - \vec{\nabla}(\bar{\sigma}) = 0 \quad (2.17)$$

Both terms can be rewritten. First we will use the chain rule of differentiations to transform the first term:

$$\vec{\nabla}(\vec{u}\vec{u}) = [\vec{\nabla}(\vec{u})]\vec{u} + (\vec{u} \cdot \vec{\nabla})\vec{u}, \quad \text{with } \vec{\nabla}(\vec{u}) = 0 \text{ (continuity)} \quad (2.18)$$

$$\bar{\sigma} = -p\bar{I} + \vec{\nabla}(\bar{\tau}) \quad (2.19)$$

For a Newtonian fluid, the viscous stress tensor holds:

$$\bar{\tau} = \mu \left[ \vec{\nabla}(\vec{u}) + (\vec{\nabla}(\vec{u}))^T \right] + \lambda [\vec{\nabla}(\vec{u})]\bar{I} \quad (2.20)$$

For incompressible flow  $\lambda[\vec{\nabla}(\vec{u})] = 0$ . Furthermore for incompressible flow and  $\mu = \text{constant}$ , equation (2.18) transforms in:

$$-p\bar{I} + \vec{\nabla}(\bar{\tau}) = -p\bar{I} + \mu(\vec{\nabla} \cdot \vec{\nabla})\vec{u} \quad (2.21)$$

This leads to the following representation of the Navier-Stokes equation:

$$\rho(\vec{u} \cdot \vec{\nabla})\vec{u} + \vec{\nabla}p - \mu(\vec{\nabla} \cdot \vec{\nabla})\vec{u} = \vec{0} \quad (2.22)$$

Now we expand the equation for  $i = 1, 2$  and dividing it by  $\rho$ :

$$i=1 \quad u \frac{\partial u}{\partial x} + v \frac{\partial u}{\partial y} = -\frac{1}{\rho} \frac{\partial p}{\partial x} + \nu \left( \frac{\partial^2 u}{\partial x^2} + \frac{\partial^2 u}{\partial y^2} \right), \quad \text{with } \frac{\mu}{\rho} = \nu \text{ (kinematic viscosity)} \quad (2.23)$$

$$i=2 \quad u \frac{\partial v}{\partial x} + v \frac{\partial v}{\partial y} = -\frac{1}{\rho} \frac{\partial p}{\partial y} + \nu \left( \frac{\partial^2 v}{\partial x^2} + \frac{\partial^2 v}{\partial y^2} \right)$$

Before continuing with the derivation of the boundary layer equations, we need to discuss another important assumption. This assumption is that the boundary layer is very thin in comparison with the length of the body. That is

$$\frac{\delta}{c} \ll 1 \quad (2.24)$$

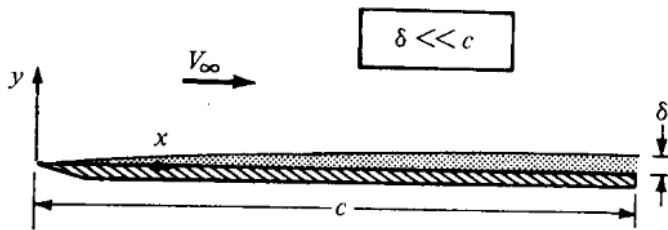


Figure 2.2 Schematic view of flat plate with boundary layer[2]

This important assumption reduces the Navier-Stokes equations yet again. Prandtl used the concept of dimensional analysis from which he found the similarity parameters. Similarity parameters are used for flows for which streamline patterns are geometrically similar and distributions of dimensionless forces, temperatures and velocities are the same when plotted against nondimensional coordinates. That is the case in this particular problem. Let us introduce the following dimensionless variables:

$$x' = \frac{x}{c}, y' = \frac{y}{\delta}, u' = \frac{u}{U_\infty}, v' = \frac{v}{V_\infty}, p' = \frac{p}{p_\infty} \quad (2.25)$$

Substituting these parameters in in the continuity equation we obtain:

$$\frac{\partial u' U_\infty}{\partial x' c} + \frac{\partial v' V_\infty}{\partial y' \delta} = \frac{\partial u'}{\partial x'} + \frac{V_\infty c}{U_\infty \delta} \frac{\partial v'}{\partial y'} = 0 \quad (2.26)$$

Assuming  $\frac{\partial u'}{\partial x'}$  and  $\frac{\partial v'}{\partial y'}$  to be of the same order, in order to balance the two terms  $V_\infty = \frac{\delta}{c} U_\infty$ . With this it follows:

$$\frac{\partial u'}{\partial x'} + \frac{\partial v'}{\partial y'} = 0 \quad (2.27)$$

Substituting the scaling in the x-momentum equation of the Navier-stokes equation we get:

$$\frac{U_\infty^2}{c} u' \frac{\partial u'}{\partial x'} + \frac{V_\infty U_\infty}{\delta} v' \frac{\partial u'}{\partial y'} = -\frac{p_\infty}{\rho c} \frac{\partial p'}{\partial x'} + \nu U_\infty \left( \frac{1}{c^2} \frac{\partial^2 u'}{\partial x'^2} + \frac{1}{\delta^2} \frac{\partial^2 u'}{\partial y'^2} \right) \quad (2.28)$$

Simplifying this equation yields:

$$u' \frac{\partial u'}{\partial x'} + \frac{V_\infty c}{U_\infty \delta} v' \frac{\partial u'}{\partial y'} = -\frac{p_\infty}{\rho U_\infty^2} \frac{\partial p'}{\partial x'} + \frac{\nu}{U_\infty c} \left( \frac{c}{\delta} \right)^2 \left( \left( \frac{\delta}{c} \right)^2 \frac{\partial^2 u'}{\partial x'^2} + \frac{\partial^2 u'}{\partial y'^2} \right) \quad (2.29)$$

Since we set  $\frac{V_\infty c}{U_\infty \delta} = 1$ , the other terms in the equation should be of the same order. This implies that  $p_\infty = \rho U_\infty^2$ . Then the equation reads:

$$u' \frac{\partial u'}{\partial x'} + v' \frac{\partial u'}{\partial y'} = -\frac{\partial p'}{\partial x'} + \frac{\nu}{U_\infty c} \left( \frac{c}{\delta} \right)^2 \left( \left( \frac{\delta}{c} \right)^2 \frac{\partial^2 u'}{\partial x'^2} + \frac{\partial^2 u'}{\partial y'^2} \right) \quad (2.30)$$

We assumed that  $\frac{\delta}{c} \ll 1$ , so this implies also that  $\left( \frac{\delta}{c} \right)^2 \ll 1$ . This has the consequence that the second term between the bracket will be much more dominant than the first term  $\left( \left| \frac{\partial^2 u}{\partial x^2} \right| \ll \left| \frac{\partial^2 u}{\partial y^2} \right| \right)$ , so we can neglect the first term. Furthermore we see that the term in front of the brackets have to be of order one, otherwise the equation makes no sense since all the other terms in the equation are order one.

$$\frac{\nu}{U_\infty c} \left( \frac{c}{\delta} \right)^2 = 1 \rightarrow \frac{\delta}{c} = \sqrt{\left( \frac{\nu}{U_\infty c} \right)} = \frac{1}{\sqrt{Re_c}} \quad (2.31)$$

Now we make another assumption for the boundary layer theory; the Reynolds number is large enough to scale with  $\delta$ . So the term in front of the brackets has the same order of magnitude as the other terms in the equation, since:

$$\frac{\nu}{U_\infty c} = \frac{1}{Re_c}, \quad \text{and} \quad \left( \frac{c}{\delta} \right)^2 = Re_c \quad (2.32)$$

The same analyse can be done for the y-momentum equation to obtain:

$$u' \frac{\partial v'}{\partial x'} + v' \frac{\partial v'}{\partial y'} = -\left( \frac{c}{\delta} \right)^2 \frac{\partial p'}{\partial y'} + \frac{\nu}{U_\infty c} \left( \frac{c}{\delta} \right)^2 \left( \left( \frac{\delta}{c} \right)^2 \frac{\partial^2 v'}{\partial x'^2} + \frac{\partial^2 v'}{\partial y'^2} \right) \quad (2.33)$$

In this equation we notice that the  $\partial p'/\partial y'$  has order  $1/\delta^2$ . Since  $\delta/c$  is very small, this implies that the  $\partial p'/\partial y'$  term is more dominant than the other terms in the equation. Therefore, we can conclude that the y-momentum equation for the boundary layer will become:

$$\frac{\partial p'}{\partial y'} = 0 \quad (2.34)$$

Transforming the equations back in terms of dimensional variables, we obtain the following equations:

$$\frac{\partial u}{\partial x} + \frac{\partial v}{\partial y} = 0 \quad (2.35)$$

$$u \frac{\partial u}{\partial x} + v \frac{\partial u}{\partial y} = -\frac{1}{\rho} \frac{\partial p}{\partial x} + \nu \left( \frac{\partial^2 u}{\partial y^2} \right) \quad (2.36)$$

$$\frac{\partial p}{\partial y} = 0 \quad (2.37)$$

The result for the y-component of the momentum equation tells us that the pressure gradient in vertical direction is zero, so the pressure in vertical direction in the boundary layer is constant. This also tells us that the pressure on the outer edge of the boundary layer is imposed directly to the surface of the body.

$$p(x) = p_e(x) \quad (2.38)$$

Now we have the boundary layer equations for a flat plate at angle of attack of zero incidence in 2D steady, incompressible flow without effects of gravity or other volumetric forces.

$$\boxed{\frac{\partial u}{\partial x} + \frac{\partial v}{\partial y} = 0, \quad u \frac{\partial u}{\partial x} + v \frac{\partial u}{\partial y} = -\frac{1}{\rho} \frac{dp_e}{dx} + \nu \left( \frac{\partial^2 u}{\partial y^2} \right), \quad \frac{\partial p_e}{\partial x} = 0} \quad (2.39)$$

The above equations are subjected to the boundary conditions at the solid surface, i.e. the no-slip condition. The no-slip condition implies that there is no velocity in the x- and y-direction at the surface of the body. Furthermore at the edge of the boundary layer the velocity in x-direction is the identical to the free stream velocity in front of the plate. So the three boundary conditions are:

$$\boxed{u(x, 0) = 0, \quad v(x, 0) = 0, \quad u(x, y \rightarrow \infty) = U_\infty} \quad (2.40)$$

Note that due to the last boundary condition and the fact that at the edge of the boundary layer the change of velocity in y-direction is zero, i.e.  $\frac{\partial u}{\partial y}(x, y \rightarrow \infty) = 0$ ;  $\frac{\partial^2 u}{\partial y^2}(x, y \rightarrow \infty) = 0$ , the x-component of the momentum equation applied at the edge of the boundary layer reduces to:

$$U_\infty \frac{dU_\infty}{dx} = -\frac{1}{\rho} \frac{dp_e}{dx} \quad (2.41)$$

## 3 Derivation of solution boundary-layer equations

### 3.1 Analytical solutions

#### 3.1.1 Blasius' Equation

In general, the laminar boundary layer equations will form a system of partial differential equations which can, in principle, be solved numerically. But it is also possible in particular conditions to work out the solution analytically in certain cases. In our case with an incompressible flow over a flat plate at zero incidence we can derive the Blasius solution. The plate starts at  $x = 0$  and extends parallel to the x-axis and will have a semi-infinite length. The free stream velocity will be constant. It follows from equation (2.41) that a constant  $U_\infty$  will result in a constant pressure at the edge of the boundary layer. This will result in the x-component of the momentum equation for the boundary layer equations:

$$u \frac{\partial u}{\partial x} + v \frac{\partial u}{\partial y} = \nu \left( \frac{\partial^2 u}{\partial y^2} \right) \quad (3.1)$$

The basic idea for obtaining an analytical result is to reduce the boundary layer equations to ordinary differential equations. To achieve this we first introduce a stream function  $\Psi(x, y)$ . We need to find a possible stream function which satisfies both the continuity equation and the Navier-Stokes equation. For satisfying the continuity equation the stream functions is defined such that:

$$u(x, y) = \frac{\partial \Psi(x, y)}{\partial y}, \quad v(x, y) = -\frac{\partial \Psi(x, y)}{\partial x} \quad (3.2)$$

Now we also need to satisfy the x-component of the momentum equation. So we substitute the stream function in (3.1). This yields:

$$\frac{\partial \Psi}{\partial y} \frac{\partial^2 \Psi}{\partial x \partial y} - \frac{\partial \Psi}{\partial x} \frac{\partial^2 \Psi}{\partial y^2} = \nu \left( \frac{\partial^3 \Psi}{\partial y^3} \right) \quad (3.3)$$

In this case there is no length scale in the flow problem: the flat plate is semi-infinite and in y-direction flow domain extends to do. This suggests the possibility of a similarity solution. For a similarity solution, a solution that depends on one variable only, such that the partial differential equation reduces to an ordinary differential equation, we want to find the  $\Psi$  to depend on a single parameter  $\eta$  only. Therefore we define:

$$\Psi(x, y) = A x^P f(\eta), \quad \eta(x, y) = B x^Q y \quad (3.4)$$

With P and Q to be determined such that equation (3.3) becomes an ordinary differential equation not depending on the x-coordinate. The terms in the x-momentum equation are successively:

$$\frac{\partial \Psi}{\partial y} = A x^P f' \cdot B x^Q = AB x^{P+Q} f' \quad (3.5)$$

$$\begin{aligned} \frac{\partial}{\partial x} \frac{\partial \Psi}{\partial y} &= AB(P+Q)x^{P+Q-1}f' + AB^2Qx^{P+2Q-1}yf'' \\ &= AB(P+Q)x^{P+Q-1}f' + ABQx^{P+Q-1}\eta f'' \end{aligned} \quad (3.6)$$

$$\frac{\partial \Psi}{\partial x} = APx^{P-1}f + ABQx^{P+Q-1}yf' = APx^{P-1}f + AQx^{P-1}\eta f' \quad (3.7)$$

$$\frac{\partial^2 \Psi}{\partial y^2} = AB^2x^{P+2Q}f'' \quad (3.8)$$

$$\frac{\partial^3 \Psi}{\partial y^3} = AB^3x^{P+3Q}f''' \quad (3.9)$$

Substituting these expressions in equation (3.3) gives:

$$ABx^{P+Q}f' \cdot (AB(P+Q)x^{P+Q-1}f' + ABQx^{P+Q-1}\eta f'') - (APx^{P-1}f + AQx^{P-1}\eta f') \cdot AB^2x^{P+2Q}f'' = vAB^3x^{P+3Q}f''' \quad (3.10)$$

This results in:

$$(P+Q)f'^2 - Pff'' = v\frac{B}{A}x^{-P+Q+1}f''' \quad (3.11)$$

For a similarity solution, equation (3.11) should be independent of  $x$ . So this means that the power of  $x$  should be zero:

$$-P+Q+1=0 \quad (3.12)$$

But there are two unknowns, so we need a second expression for  $P$  and  $Q$  in order to obtain the solution. For this we consider the boundary conditions, equation (2.40). The first boundary condition is  $u(x,0) = 0$ . Substituting this with the new parameters:

$$u(x,0) = \frac{\partial\Psi(x,0)}{\partial y} = ABx^{P+Q}f'(0) = 0 \quad (3.13)$$

$A$  nor  $B$  will not be zero, this is a trivial solution. So this means that  $f'(0) = 0$ . The second boundary equation is  $v(x,0) = 0$ . This results in:

$$v(x,0) = -\frac{\partial\Psi(x,0)}{\partial x} = -(APx^{P-1}f(0) + ABQx^{P+Q-1}yf'(0)) = 0 \quad (3.14)$$

Since  $f'(0) = 0$  already, it follows that  $f(0) = 0$ . The last boundary condition is  $u(x,\infty) = U_\infty$ . When we substitute this we obtain:

$$u(x,\infty) = \frac{\partial\Psi(x,\infty)}{\partial y} = ABx^{P+Q}f'(\infty) = U_\infty \quad (3.15)$$

For the same reason at equation (3.12), we can state this boundary condition should be independent of  $x$ , so that:

$$P+Q=0 \quad (3.16)$$

We now have two equations - (3.12) and (3.16) - for  $P$  and  $Q$ . So we find:

$$P = \frac{1}{2}, \quad Q = -\frac{1}{2} \quad (3.17)$$

We still need an expression for  $A$  and  $B$ . Considering equation (3.11) we choose for convenience:

$$v\frac{B}{A} = 1 \quad (3.18)$$

And from equation (3.15) we set:

$$AB = U_\infty, \quad \text{so that } f'(\infty) = 1 \quad (3.19)$$

Equations (3.18) and (3.19) give us the opportunity to find the parameters  $A$  and  $B$ :

$$A = \sqrt{U_\infty v}, \quad B = \sqrt{\frac{U_\infty}{v}} \quad (3.20)$$

Substituting these parameters in equation (3.11) and we obtain the Blasius equation for  $f(\eta)$ :

$$f''' + \frac{1}{2}ff'' = 0, \quad \text{with } \Psi(x, y) = \sqrt{U_\infty vx} f(\eta), \quad \text{and } \eta = \sqrt{\frac{U_\infty}{vx}} y \quad (3.21)$$

Note that  $f$  and  $\eta$  are dimensionless. The three boundary conditions required for the third-degree ordinary differential equation to solve are:

$$f(0) = 0, \quad f'(0) = 0, \quad f'(\infty) = 1 \quad (3.22)$$

Let us look more closely to this result. We went from the partial differential equation of the x-momentum, equation (2.39), to an ordinary differential equation for  $f(\eta)$ . Since we found the stream function, we can use the definition of the stream function of equation (3.2) to obtain the velocity of the flow in x-direction :

$$u(x, y) = \frac{\partial \Psi(x, y)}{\partial y} = ABx^{P+Q}f' = U_\infty f'(\eta) \quad (3.23)$$

For the velocity of the flow in y-direction it follows:

$$v(x, y) = -\frac{\partial \Psi(x, y)}{\partial x} = APx^{P-1}f + AQx^{P-1}\eta f' = \frac{1}{2}U_\infty Re_x^{-1/2}(\eta f' - f) \quad (3.24)$$

This means that since the Blasius solution is only depending on  $f(\eta)$ , the velocity in x-direction  $u$  depends on  $\eta$  only. The vertical component of the velocity is a function of  $\eta$  times a scaling factor proportional to  $Re_x^{-1/2}$ .

### 3.1.2 Shooting method

To solve the Blasius equation, i.e. a third-order nonlinear ordinary differential equation, we rewrite the equation to three first-order ordinary differential equations. We then have three so-called initial value problems which can be solved. The Blasius equation is rewritten in such a way that it is an equation involving only a first-derivative:

$$\frac{df}{d\eta} = f', \quad \text{with } f(0) = 0 \quad (3.25)$$

$$\frac{df'}{d\eta} = f'', \quad \text{with } f'(0) = 0, \quad \text{and } f'(\infty) = 1 \quad (3.26)$$

$$\frac{df''}{d\eta} = -\frac{1}{2}ff'', \quad \text{with } f''(0) = ? \quad (3.27)$$

The problem now is the missing third initial value  $f''(0)$ . But since we know  $f'(\infty) = 1$ , we can use the shooting method. The shooting method is a procedure using a guess for the third, missing, initial value, carrying out the calculations and comparing the result with the result for  $f'(\infty)$  which should be  $f'(\infty) = 1$ . To solve the initial value problem use is made of the Euler forward method. The goal of this technique is to approximate the first derivative in the differential equation. It is based on finding the next value of a graph by adding the old value plus the derivative of the curve at the old value times an arbitrary step size. This numerical method works well for small enough chosen step sizes. So Euler's forward method for the three differential equations above results in:

$$f_{i+1} = f_i + f'_i dn \quad (3.28)$$

$$f'_{i+1} = f'_i + f''_i dn \quad (3.29)$$

$$f''_{i+1} = f''_i - \frac{1}{2}f_i f''_i dn \quad (3.30)$$

### 3.1.3 Results

#### 3.1.3.1 Velocity profile for flat plate

Using the guess for  $f''(0)$  we can evaluate the three equations above and repeat this for  $i = 0, 1, \dots$  up to large values of  $\eta$  until  $f'(\eta)$  does not change anymore. After this we check whether the result of the Euler forward method for high values of  $\eta$  gives  $f''_{\infty} \approx f''(\infty) = 1$ . If not, we choose another value for  $f''(0)$ , repeat the calculations etc.. Using the shooting method we find:

$$f''(0) = 0.332 \quad (3.31)$$

The solutions for the components of the dimensionless velocity components in x- and y-direction are plotted in figure 3.1 and so are the functions  $f(\eta)$  and  $f''(\eta)$ . Consider the plot of  $f'(\eta)$  which corresponds to the distribution of the dimensionless x-component of the velocity;  $\eta$  is dependent on  $x$  and  $y$ . So at two different  $x$ -positions along the flat plate the velocity profile is the same. This means that in order to have the same value of  $\eta$ ,  $y$  needs to compensate the change in  $x$ . So along the plate the boundary layer will grow in vertical direction due to the increasing  $x$  in such a way that the distribution remains identical in terms of  $\eta$ . Such a result is called a self-similar solution.

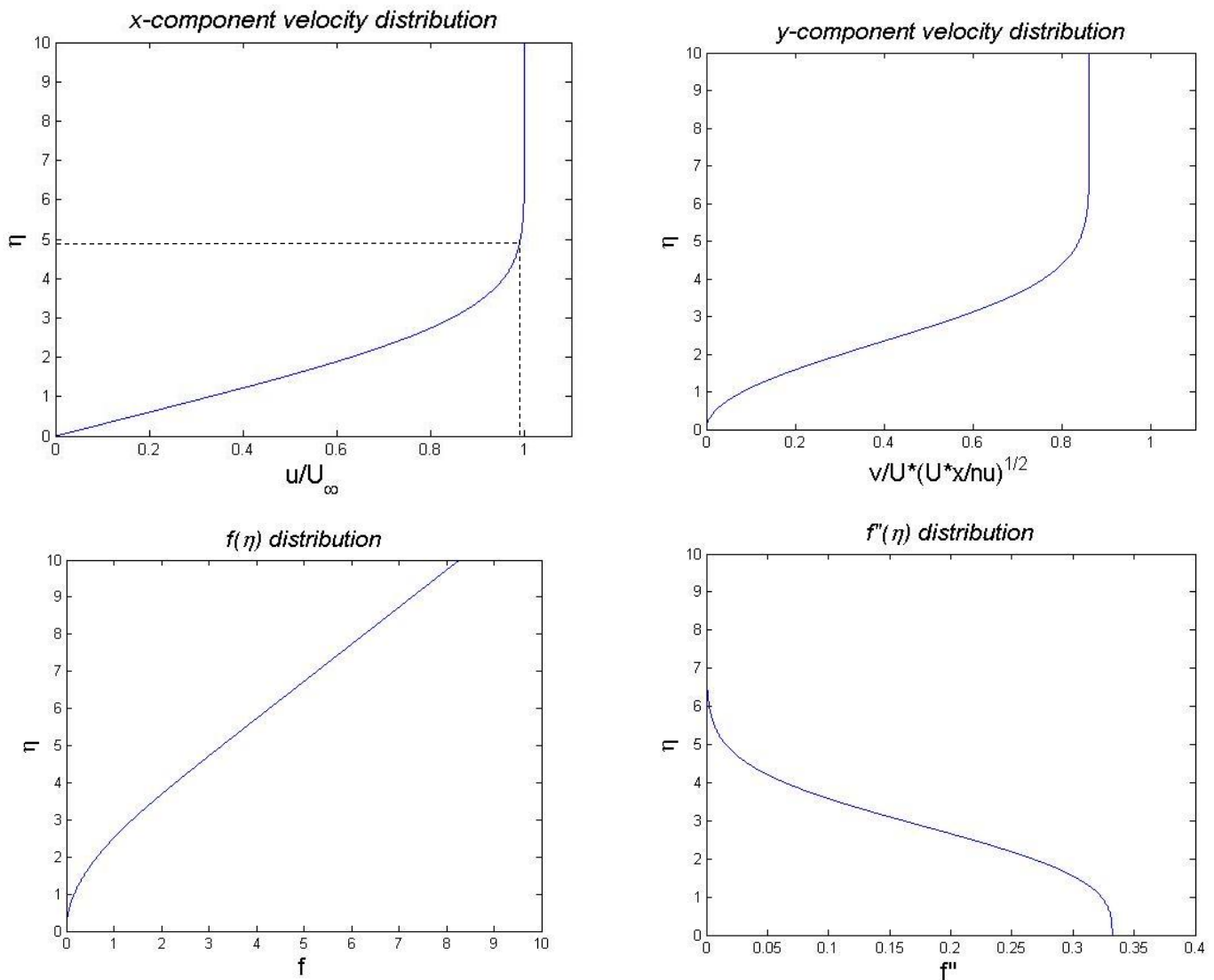


Figure 3.1 Blasius' solution for the self-similar velocity distribution in a laminar boundary layer along a flat plate at zero angle of attack

### 3.1.3.2 Boundary layer thickness

When we examine the plot for  $f'$  against  $\eta$  we choose the  $\eta$  for which  $u = 0.99U_\infty$ . We assume that at this location the edge of the boundary layer has been reached. In our calculations  $u/U_\infty$  reaches 0.99 at  $\eta = 4.9$ . With this information we find:

$$\eta = \sqrt{\frac{U_\infty}{\nu x}} y \rightarrow \delta(x) = \frac{4.9x}{\sqrt{Re_x}} = c \frac{4.9}{\sqrt{Re_c}} \left(\frac{x}{c}\right)^{\frac{1}{2}} \quad (3.32)$$

$$\frac{\delta(x)}{c} = \frac{4.9}{(Re_c)^{\frac{1}{2}}} \left(\frac{x}{c}\right)^{\frac{1}{2}} \quad (3.33)$$

Let us examine this result. We find that the boundary layer thickness is proportional to the square root of the local dimensionless coordinate and inversely proportional to the square root of the Reynolds number  $Re_c$ . Therefore, the boundary layer thickness is proportional to the square root of the x-position along the surface of the plate. This leads to the conclusion that the boundary layer over a flat plate grows parabolically with the distance from the leading edge, i.e. like  $\left(\frac{x}{c}\right)^{\frac{1}{2}}$ , and that with increasing Reynolds number  $Re_c$  the boundary layer will be thinned.

### 3.1.3.3 Skin-friction coefficient[3]

More results can be derived from this approach of solving the Blasius equation. Let us introduce the skin friction of the flat plate. Skin friction arises when a fluid flows over a solid surface. The fluid is in contact with the surface of the body, resulting in a friction force exerted on the surface. The friction force per unit area is called the wall shear stress. The shear stress for most common fluids, i.e. so-called Newtonian fluids, depends on the dynamic viscosity and the gradient of the velocity:

$$\tau_s = \mu \left. \frac{\partial u}{\partial y} \right|_{y=0} \quad (3.34)$$

Since we know  $u(x, y) = U_\infty f'(\eta)$  from equation (3.23) we can rewrite the equation for the wall shear stress, using:

$$\frac{\partial u}{\partial y} = U_\infty \frac{df'(\eta)}{d\eta} \frac{\partial \eta}{\partial y} = U_\infty f'' \sqrt{\frac{U_\infty}{\nu x}} \quad (3.35)$$

As:

$$\tau_w = \mu \left. \frac{\partial u}{\partial y} \right|_{y=0} = \mu U_\infty \sqrt{\frac{U_\infty}{\nu x}} f''(0) = \rho U_\infty^2 Re_x^{-1/2} f''(0) \quad (3.36)$$

The dimensionless skin-friction is called the local skin-friction coefficient. This is defined as:

$$c_f \equiv \frac{\tau_w}{\frac{1}{2} \rho U_\infty^2} = \frac{2}{(Re_x)^{\frac{1}{2}}} f''(0) = \frac{2}{(Re_c)^{\frac{1}{2}}} \left(\frac{x}{c}\right)^{-\frac{1}{2}} f''(0) \quad (3.37)$$

From the shooting method we found for  $f''(0)$  the numerical value of 0.332, so with this, equation (3.37) transforms in:

$$c_f(x) = \frac{2f''(0)}{(Re_x)^{\frac{1}{2}}} = \frac{0.664}{(Re_x)^{\frac{1}{2}}} = \frac{0.664}{(Re_c)^{\frac{1}{2}}} \left(\frac{x}{c}\right)^{-\frac{1}{2}} \quad (3.38)$$

So the skin friction coefficient decreases as  $\left(\frac{x}{c}\right)^{-\frac{1}{2}}$  with increasing distance from the leading edge. For the skin friction coefficient of the entire plate we use the following equation:

$$C_f \equiv \frac{1}{c} \int_0^c c_f dx = \frac{0.664}{c \sqrt{\frac{U_\infty}{\nu}}} \int_0^c x^{-\frac{1}{2}} dx = \frac{1.328}{(Re_c)^{\frac{1}{2}}} \quad (3.39)$$

This shows that with increasing  $Re_c$  the skin friction coefficient of the plate decreases.

### 3.1.3.4 Displacement thickness

This frequently used boundary layer property describes the difference between the case with hypothetical flow over a flat plate without a boundary layer and the actual flow with a boundary layer.

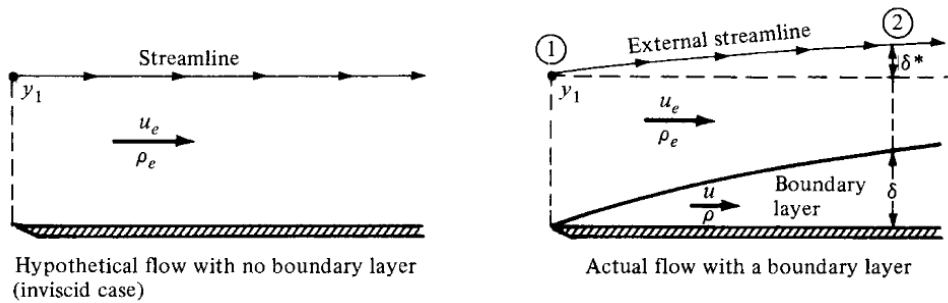


Figure 3.1 Schematic view explaining the influence of the boundary layer on external streamlines [2]

Because of the presence of a boundary layer, the streamlines passing through point  $y_1$  are deflected upward over a distance  $\delta^*$ . We can calculate this distance by equating the mass flow between the solid surface and the external streamline at point 1:

$$\dot{m} = \int_0^{y_1} \rho_e u_e dy \quad (3.40)$$

And similarly at point 2:

$$\dot{m} = \int_0^{y_1} \rho u dy + \rho_e u_e \delta^* \quad (3.41)$$

The mass flow through the surface at point 1 and through the surface at point 2 are equal since the streamline passes from point 1 to point 2. This means:

$$\int_0^{y_1} \rho_e u_e dy = \int_0^{y_1} \rho u dy + \rho_e u_e \delta^* \quad (3.42)$$

We obtain from this equation the displacement thickness  $\delta^*$ :

$$\delta^*(x) = \frac{\int_0^{y_1} (\rho_e u_e - \rho u) dy}{\rho_e u_e} = \int_0^{y_1} \left(1 - \frac{\rho u}{\rho_e u_e}\right) dy \quad (3.43)$$

We now return to the situation for an incompressible flow ( $\rho = \text{constant} \rightarrow \rho = \rho_e$ ) and the velocity at the edge of the boundary layer is  $u_e = U_\infty$ . For this situation the displacement thickness becomes:

$$\delta^*(x) = \int_0^{y_1} \left(1 - \frac{u(x,y)}{U_\infty}\right) dy \quad (3.44)$$

We can transform this equation in terms of the transformed variables  $\eta$  and  $f'(\eta)$  from equation (3.21) and (3.23). This results in:

$$\eta_1 = \sqrt{\frac{U_\infty}{\nu x}} y_1 \rightarrow y_1 = \eta_1 \sqrt{\frac{\nu x}{U_\infty}} = \eta_1 x \sqrt{\frac{\nu}{U_\infty x}} = \frac{\eta_1 x}{\sqrt{Re_x}} \quad (3.45)$$

$$f'(\eta) = \frac{u}{U_\infty} \quad (3.46)$$

Substituting this in equation (3.44), results in:

$$\delta^*(x) = \frac{x}{\sqrt{Re_x}} \int_0^{\eta_1} (1 - f'(\eta)) d\eta = \frac{(\eta_1 - f(\eta_1))x}{\sqrt{Re_x}}, \quad \text{since } f(0) = 0 \quad (3.47)$$

When we consider the numerical result of  $\eta_1 - f(\eta_1)$ , we see that for all values above  $\eta = 4.9$  the result is 1.727. So when we reach the point of the edge of the boundary layer  $\eta_1 - f(\eta_1) = \text{constant}$ .

This results in an equation for the displacement thickness:

$$\delta^*(x) = \frac{1.727x}{(Re_x)^{\frac{1}{2}}} \rightarrow \frac{\delta^*(x)}{c} = \frac{1.727}{(Re_c)^{\frac{1}{2}}} \left(\frac{x}{c}\right)^{\frac{1}{2}} \quad (3.48)$$

We see that also the displacement thickness is proportional to the square root of the x-position. This agrees with the definition of the displacement thickness, it is impossible to have a growing boundary layer and a decreasing displacement thickness. Now we can express the boundary layer thickness in terms of the displacement thickness:

$$\frac{\delta^*}{\delta} = \frac{\frac{1.727x}{\sqrt{Re_x}}}{\frac{4.9x}{\sqrt{Re_x}}} = 0.35 \rightarrow \delta^*(x) = 0.35\delta(x) \quad (3.49)$$

This result tells us that the displacement thickness is about 3 times smaller than the boundary layer thickness itself.

### 3.1.3.5 Momentum Thickness

Another frequently used characteristic of a boundary layer is the momentum thickness. This property gives us an index proportional to the decrement of the flux of momentum due to the presence of the boundary layer. We will derive the momentum thickness with the help of figure 3.2.

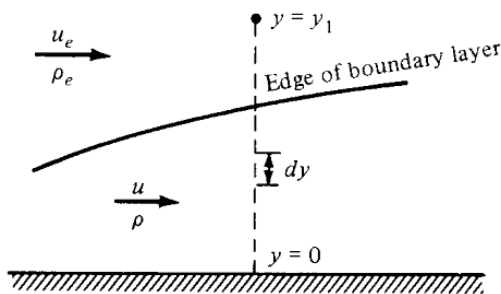


Figure 3.2 Schematic view explaining the definition of momentum thickness [2]

We consider a mass flux across a segment  $dy$  of  $dm = \rho u dy$ . Then consider the momentum flux (mass flux times the velocity) at segment  $dy$  with and without the presence of the boundary layer. First the momentum flux with the boundary layer:

$$dM = dm u = \rho u^2 dy \quad (3.50)$$

And then without the boundary layer:

$$dM = dm u_e = (\rho u dy) u_e \quad (3.51)$$

Integrating over the boundary layer, from 0 and  $y_1$  we obtain the total momentum flux. When we subtract equation (3.50) and (3.51) and take the integral, we obtain the total decrement in momentum flux:

$$\dot{M} = \int_0^{y_1} \rho u (u_e - u) dy \quad (3.52)$$

Now we assume that the missing momentum flux is the product of  $\rho_e u_e^2$  and the height  $\theta$ , and compare these two definitions for the missing momentum flux due the presence of the boundary layer:

$$\rho_e u_e^2 \theta = \int_0^{y_1} \rho u (u_e - u) dy \quad (3.53)$$

We obtain from this equation the momentum thickness  $\theta$ :

$$\theta(x) = \frac{\left( \int_0^{y_1} \rho u (u_e - u) dy \right)}{\rho_e u_e^2} = \int_0^{y_1} \frac{\rho u}{\rho_e u_e} \left( 1 - \frac{u}{u_e} \right) dy \quad (3.54)$$

Again let us return to the situation where we have an incompressible flow ( $\rho = \text{constant} \rightarrow \rho = \rho_e$ ) and the velocity at the edge of the boundary layer is  $u_e = U_\infty$ . Then the momentum thickness becomes:

$$\theta(x) = \int_0^{y_1} \frac{u(x, y)}{U_\infty} \left( 1 - \frac{u(x, y)}{U_\infty} \right) dy \quad (3.55)$$

Also here we will use the similarity variables  $\eta$  and  $f'(\eta)$  from equation (3.21) and (3.23). This results in:

$$\theta(x) = \frac{x}{\sqrt{Re_x}} \int_0^{\eta_1} f'(\eta) (1 - f'(\eta)) d\eta \quad (3.56)$$

The equation in the integral  $f'(\eta)(1 - f'(\eta))$  cannot be integrated analytically. However, for  $\eta > 4.9$   $f'(\eta)$  will not change anymore and will be equal to 1.0. The numerical result of the integral is 0.664. So we obtain the momentum thickness in our case:

$$\theta(x) = \frac{0.664x}{(Re_x)^{\frac{1}{2}}} \rightarrow \frac{\theta(x)}{c} = \frac{0.664}{(Re_c)^{\frac{1}{2}}} \left( \frac{x}{c} \right)^{\frac{1}{2}} \quad (3.57)$$

So also the momentum thickness is proportional to  $\left( \frac{x}{c} \right)^{\frac{1}{2}}$ . Therefore, also the momentum thickness grows with the square root of the x-position on the flat plate. The momentum thickness can be expressed in terms of the boundary-layer thickness and the displacement thickness:

$$\theta(x) = 0.13\delta(x), \quad \theta(x) = 0.38\delta^*(x) \quad (3.58)$$

## 3.2 Approximation solutions

The boundary layer equations are a set of partial differential equations which we have to solve to obtain results like the Blasius equation. In this chapter we will not obtain the exact solution, but we will approximate the solution of the boundary layer equations.

### 3.2.1 Momentum-Integral Equation

Approximation solutions of the boundary layer equations can be obtained from the Momentum-Integral Equation in combination with making an educated guess for the velocity profile. First we will obtain the Momentum-Integral Equation[4]. We start with the boundary layer equations from equation (3.39) and the definition for the pressure distribution from equation (3.41)

$$\begin{aligned} \frac{\partial u}{\partial x} + \frac{\partial v}{\partial y} &= 0 \\ u \frac{\partial u}{\partial x} + v \frac{\partial u}{\partial y} &= -\frac{1}{\rho} \frac{dp_e}{dx} + v \left( \frac{\partial^2 u}{\partial y^2} \right) \\ U_\infty \frac{dU_\infty}{dx} &= -\frac{1}{\rho} \frac{dp_e}{dx} \end{aligned} \quad (3.59)$$

Let us rewrite the continuity equation in order to obtain the velocity in y-direction  $v$  inside the boundary layer:

$$\frac{\partial v}{\partial y} = -\frac{\partial u}{\partial x} \rightarrow v(x, y) = \int_0^y \left( -\frac{\partial u}{\partial x} \right) dy' = -\frac{\partial}{\partial x} \int_0^y u(x, y') dy' \quad (3.60)$$

Where we used  $v(x, 0) = 0$ . Here  $y$  is an arbitrary value. Also, we rewrite the x-momentum equation using (3.59) like:

$$u \frac{\partial u}{\partial x} + v \frac{\partial u}{\partial y} = U_\infty \frac{dU_\infty}{dx} + v \left( \frac{\partial^2 u}{\partial y^2} \right) \quad (3.61)$$

Now substitute (3.60) in (3.61) in order to obtain:

$$u \frac{\partial u}{\partial x} + \frac{\partial u}{\partial y} \int_0^y \left( -\frac{\partial u}{\partial x} \right) dy - U_\infty \frac{dU_\infty}{dx} = v \left( \frac{\partial^2 u}{\partial y^2} \right) \quad (3.62)$$

Integrate both sides, with  $h$  an arbitrary location in the free stream where  $u = U_\infty$  and  $\partial u / \partial y = 0$ :

$$\int_0^h \left( u \frac{\partial u}{\partial x} + \frac{\partial u}{\partial y} \int_0^y \left( -\frac{\partial u}{\partial x} \right) dy - U_\infty \frac{dU_\infty}{dx} \right) dy = \int_0^h \left( v \left( \frac{\partial^2 u}{\partial y^2} \right) \right) dy \quad (3.63)$$

We can carry out the integral for the term on the right side of the equation:

$$\int_0^h \left( v \left( \frac{\partial^2 u}{\partial y^2} \right) \right) dy = v \left( \frac{\partial u}{\partial y} \Big|_{y=h} - \frac{\partial u}{\partial y} \Big|_{y=0} \right) = -v \frac{\partial u}{\partial y} \Big|_{y=0} \quad (3.64)$$

It follows from equation (3.34) that the partial derivative can be rewritten to obtain:

$$\tau_s = \mu \frac{\partial u}{\partial y} \Big|_{y=0} \rightarrow \frac{\partial u}{\partial y} \Big|_{y=0} = \frac{\tau_s}{\mu} \quad (3.65)$$

Taking this into account the right side of equation (3.64) yields:

$$-v \frac{\tau_s}{\mu} = -\frac{\tau_s}{\rho} \quad (3.66)$$

Returning to equation (3.63), we can rewrite the second term inside the integral with the method of integration by parts:

$$\begin{aligned} \int_0^h \left[ \left( \int_0^y -\frac{\partial u}{\partial x} dy' \right) \cdot \frac{\partial u}{\partial y} \right] dy &= \left[ \left( \int_0^y -\frac{\partial u}{\partial x} dy' \right) \cdot u \right]_0^h - \int_0^h -\frac{\partial u}{\partial x} u dy \\ &= \int_0^h \left( -U_\infty \frac{\partial u}{\partial x} + u \frac{\partial u}{\partial x} \right) dy \end{aligned} \quad (3.67)$$

Substituting equations (3.66) and (3.67) in equation (3.63), we get:

$$\int_0^h \left( 2u \frac{\partial u}{\partial x} - U_\infty \frac{\partial u}{\partial x} - U_\infty \frac{dU_\infty}{dx} \right) dy = -\frac{\tau_s}{\rho} \quad (3.68)$$

Now we need some more mathematical rewriting to derive the Momentum-Integral Equation:

$$\begin{aligned} &\int_0^h \left( 2u \frac{\partial u}{\partial x} - U_\infty \frac{\partial u}{\partial x} - U_\infty \frac{dU_\infty}{dx} \right) dy \\ &= \int_0^h \left( 2u \frac{\partial u}{\partial x} - U_\infty \frac{\partial u}{\partial x} - u \frac{dU_\infty}{dx} + u \frac{dU_\infty}{dx} - U_\infty \frac{dU_\infty}{dx} \right) dy \\ &= \int_0^h \left( 2u \frac{\partial u}{\partial x} - U_\infty \frac{\partial u}{\partial x} - u \frac{dU_\infty}{dx} \right) dy + \int_0^h \left( u \frac{dU_\infty}{dx} - U_\infty \frac{dU_\infty}{dx} \right) dy \\ &= \int_0^h \left( \frac{\partial}{\partial x} (u^2) - \frac{\partial}{\partial x} (U_\infty u) \right) dy + \frac{dU_\infty}{dx} \int_0^h (u - U_\infty) dy \\ &= \int_0^h \left( \frac{\partial}{\partial x} (u(u - U_\infty)) \right) dy + \frac{dU_\infty}{dx} \int_0^h (u - U_\infty) dy \\ &= \frac{\partial}{\partial x} \int_0^h u(u - U_\infty) dy + \frac{dU_\infty}{dx} \int_0^h (u - U_\infty) dy \end{aligned} \quad (3.69)$$

We recall the definitions of the displacement thickness and the momentum thickness:

$$\begin{aligned} \delta^* &= \int_0^{y_1} \left( 1 - \frac{u}{U_\infty} \right) dy \quad \rightarrow \quad U_\infty \delta^* = \int_0^{y_1} (U_\infty - u) dy \\ \theta &= \int_0^{y_1} \frac{u}{U_\infty} \left( 1 - \frac{u}{U_\infty} \right) dy \quad \rightarrow \quad U_\infty^2 \theta = \int_0^{y_1} u (U_\infty - u) dy \end{aligned} \quad (3.70)$$

Now we have gathered all the information for the Momentum-Integral Equation. We will multiply equation (3.69) with -1, and substitute equations (3.70), and we find the Momentum-Integral Equation for plane, incompressible boundary layers:

$$\frac{d}{dx} (U_\infty^2 \theta) + \delta^* U_\infty \frac{dU_\infty}{dx} = \frac{\tau_s}{\rho} \quad (3.71)$$

### 3.2.2 Approximation velocity profile

The Momentum-Integral Equation initially contains too many unknowns to solve the equation. We need to approximate the velocity profile and assume that this velocity profile has the same shape everywhere in the boundary layer, i.e. is self-similar. We will begin with a velocity profile depending on  $\eta$ , which is a dimensionless parameter ( $\eta = \frac{y}{\delta}$ ). Note that this  $\eta$  is different from the one used in section 3.1. We will work out all the results for a cubic velocity profile and then for a quartic velocity profile [5].

#### 3.2.2.1 Cubic velocity profile

We take the following cubic velocity profile:

$$u(\eta) = U_\infty(A_0 + A_1\eta + A_2\eta^2 + A_3\eta^3) \quad (3.72)$$

We have 4 yet unknown constants ( $A_{0-3}$ ). To find these constants, we need 4 boundary conditions. On the plate ( $\eta = 0$ ) due to the no-slip condition the velocity has to be zero. But also the derivative with respect to  $x$  of the velocity in  $x$ -direction are zero, so this transforms the  $x$ -momentum boundary layer equation (3.39) applied at  $y = 0$ , with the definition for the pressure distribution from equation (3.41) in:

$$v \left( \frac{\partial^2 u}{\partial y^2} \right)_{y=0} = -U_\infty \frac{dU_\infty}{dx} \quad (3.73)$$

So we obtain 2 boundary conditions for  $\eta = 0$ . The other boundary conditions can be found at the edge of the boundary layer ( $\eta = 1$ ). There the velocity is equal to the free stream velocity and the first derivative, second derivative, and so on with respect to  $y$  are zero on the edge of the boundary layer. So the 4 boundary conditions for the cubic velocity profile are:

$$\begin{array}{lll} \eta = 0 & u(\eta) = 0 & \frac{\partial^2 u}{\partial y^2} = -\frac{U_\infty}{v} \frac{dU_\infty}{dx} \\ \eta = 1 & u(\eta) = U_\infty & \frac{\partial u}{\partial y} = 0 \end{array} \quad (3.74)$$

To obtain the unknown constants in the velocity profile we substitute the boundary conditions in the equation for the velocity. We present the results from this procedure in matrix form:

$$\begin{bmatrix} 1 & 0 & 0 & 0 \\ 0 & 0 & X & 0 \\ 1 & 1 & 1 & 1 \\ 0 & 1 & 2 & 3 \end{bmatrix} \begin{bmatrix} A_0 \\ A_1 \\ A_2 \\ A_3 \end{bmatrix} = \begin{bmatrix} 0 \\ 1 \\ 1 \\ 0 \end{bmatrix} \quad \text{with } X = -\frac{\delta^2}{2v} \frac{dU_\infty}{dx} \quad (3.75)$$

This results in the following:

$$A_0 = 0, \quad A_1 = \frac{3}{2} + \frac{\delta^2}{4v} \frac{dU_\infty}{dx}, \quad A_2 = -\frac{\delta^2}{2v} \frac{dU_\infty}{dx}, \quad A_3 = -\frac{1}{2} + \frac{\delta^2}{4v} \frac{dU_\infty}{dx} \quad (3.76)$$

Substituting these results in the equation for the velocity we get:

$$u(\eta) = U_\infty \left( \frac{3}{2}\eta - \frac{1}{2}\eta^3 + \lambda(\eta - 2\eta^2 + \eta^3) \right), \quad \text{with } \lambda = \frac{\delta^2}{4v} \frac{dU_\infty}{dx} \quad (3.77)$$

Here  $\lambda$  is a dimensionless velocity gradient.

### 3.2.2.2 Quartic velocity profile

The same procedure can be carried out for a quartic velocity profile:

$$u(\eta) = U_\infty(A_0 + A_1\eta + A_2\eta^2 + A_3\eta^3 + A_4\eta^4) \quad (3.78)$$

Here we have 5 unknown constants, so we need 5 boundary conditions. The first 3 boundary conditions are the same as for the cubic profile. The 4<sup>th</sup> boundary condition gives expressions for the first and second derivative of  $u$  with respect to  $y$ . To summarize:

$$\begin{array}{llll} \eta = 0 & u(\eta) = 0 & \frac{\partial^2 u}{\partial y^2} = -\frac{U_\infty}{v} \frac{dU_\infty}{dx} & \\ \eta = 1 & u(\eta) = U_\infty & \frac{\partial u}{\partial y} = 0 & \frac{\partial^2 u}{\partial y^2} = 0 \end{array} \quad (3.79)$$

Substitution of these boundary conditions in the quartic velocity profile yields:

$$\begin{bmatrix} 1 & 0 & 0 & 0 & 0 \\ 0 & 0 & \frac{1}{X} & 0 & 0 \\ 1 & 1 & 1 & 1 & 1 \\ 0 & 1 & 2 & 3 & 4 \\ 0 & 0 & 2 & 6 & 12 \end{bmatrix} \begin{bmatrix} A_0 \\ A_1 \\ A_2 \\ A_3 \\ A_4 \end{bmatrix} = \begin{bmatrix} 0 \\ 1 \\ 1 \\ 0 \\ 0 \end{bmatrix}, \quad \text{with } X = -\frac{\delta^2}{2\nu} \frac{dU_\infty}{dx} \quad (3.80)$$

Solving this system of equations gives:

$$A_0 = 0, A_1 = 2 + \frac{\delta^2}{6\nu} \frac{dU_\infty}{dx}, A_2 = -\frac{\delta^2}{2\nu} \frac{dU_\infty}{dx}, A_3 = -2 + \frac{\delta^2}{2\nu} \frac{dU_\infty}{dx}, A_4 = 1 - \frac{\delta^2}{6\nu} \frac{dU_\infty}{dx} \quad (3.81)$$

Filling these results in the quartic velocity profile we obtain:

$$u(\eta) = U_\infty(2\eta - 2\eta^3 + \eta^4 + \hat{\lambda}(\eta - 3\eta^2 + 3\eta^3 - \eta^4)), \quad \text{with } \hat{\lambda} = \frac{\delta^2}{6\nu} \frac{dU_\infty}{dx} \quad (3.82)$$

Again  $\hat{\lambda}$  is a dimensionless velocity gradient.

### 3.2.3 Results

The two velocity profiles are substituted in the Momentum-Integral Equation. For this we need the displacement thickness, the momentum thickness and the wall shear stress. Then, the Momentum-Integral Equation will only depend on the boundary layer thickness  $\delta(x)$ . Subsequently we find the displacement thickness, the momentum thickness and the friction coefficient.

#### 3.2.3.1 Cubic velocity profile

Let us first substitute the cubic velocity profile in the displacement thickness, the momentum thickness and the wall shear stress. The displacement thickness becomes:

$$\begin{aligned} \delta^* &= \int_0^{y_1} \left(1 - \frac{u(x,y)}{U_\infty}\right) dy \\ &= \delta \int_0^1 \left(1 - \frac{u(\eta)}{U_\infty}\right) d\eta, \quad \text{with } dy = \delta d\eta \\ &= \delta \left(\frac{3}{8} - \frac{1}{12} \lambda\right), \quad \text{with } \lambda = \frac{\delta^2}{4\nu} \frac{dU_\infty}{dx} \end{aligned} \quad (3.83)$$

And the momentum thickness:

$$\begin{aligned} \theta &= \int_0^{y_1} \frac{u(x,y)}{U_\infty} \left(1 - \frac{u(x,y)}{U_\infty}\right) dy = \delta \int_0^1 \frac{u(\eta)}{U_\infty} \left(1 - \frac{u(\eta)}{U_\infty}\right) d\eta \\ &= \delta \left(\frac{39}{280} - \frac{1}{140} \lambda - \frac{1}{105} \lambda^2\right) \end{aligned} \quad (3.84)$$

And finally the wall shear stress:

$$\tau_s = \mu \left. \frac{\partial u(y)}{\partial y} \right|_{y=0} = \mu \left. \left( \frac{du(\eta)}{d\eta} \frac{\partial \eta}{\partial y} \right) \right|_{\eta=0} = \frac{\mu U_\infty}{\delta} \left( \frac{3}{2} + \lambda \right) \quad (3.85)$$

For the flow over a flat plate the free stream velocity is constant. This implies that the derivative of the free stream velocity is zero and therefore  $\lambda$  is zero. Now we can find the solution of the ordinary differential equation for  $\delta(x)$  analytically. Substituting all the parameters in the Momentum-Integral Equation yields:

$$\frac{d}{dx}(\delta) = \frac{140}{13} \frac{\nu}{U_\infty} \frac{1}{\delta} \quad (3.86)$$

We can rewrite this equation on the following manner:

$$\frac{d}{dx}(\delta) = \frac{140}{13} \frac{\nu}{U_\infty} \frac{1}{\delta} \rightarrow \frac{1}{2} \frac{d\delta^2}{dx} = \frac{140}{13} \frac{\nu}{U_\infty} \quad (3.87)$$

Integrating from the leading edge, where we take  $\delta = 0$ , to  $x$  gives:

$$\frac{1}{2} \delta(x)^2 = \frac{140}{13} \frac{\nu x}{U_\infty} \quad (3.88)$$

So now we found an equation for the boundary layer thickness:

$$\delta(x) = \sqrt{\frac{280}{13}} \sqrt{\frac{\nu x}{U_\infty}} = \frac{4.64x}{(Re_x)^{\frac{1}{2}}} \rightarrow \frac{\delta(x)}{c} = \frac{4.64}{(Re_c)^{\frac{1}{2}}} \left(\frac{x}{c}\right)^{\frac{1}{2}} \quad (3.89)$$

With this expression for the boundary layer thickness, we can find the displacement thickness, the momentum thickness and the total skin friction coefficient by putting this result in the equations (3.83), (3.84) and (3.85).

$$\delta^*(x) = \frac{3}{8} \delta \rightarrow \frac{\delta^*(x)}{c} = \frac{1.74}{(Re_c)^{\frac{1}{2}}} \left(\frac{x}{c}\right)^{\frac{1}{2}} \quad (3.90)$$

$$\theta(x) = \frac{39}{280} \delta \rightarrow \frac{\theta(x)}{c} = \frac{0.646}{(Re_c)^{\frac{1}{2}}} \left(\frac{x}{c}\right)^{\frac{1}{2}} \quad (3.91)$$

$$C_f = \frac{1}{c} \int_0^c \frac{\tau_s}{\frac{1}{2} \rho U_\infty^2} dx = \frac{1}{c} \int_0^c \frac{0.646}{\sqrt{Re_x}} dx = \frac{1.292}{(Re_c)^{\frac{1}{2}}} \quad (3.92)$$

### 3.2.3.2 Quartic velocity profile

We follow the same procedure for the quartic velocity profile. We first find the displacement thickness, the momentum thickness and the wall shear stress by substituting the quartic velocity profile in the definition for these quantities:

$$\delta^*(x) = \delta(x) \left( \frac{3}{10} - \frac{1}{20} \hat{\lambda} \right), \quad \text{with } \hat{\lambda} = \frac{\delta^2}{6\nu} \frac{dU_\infty}{dx} \quad (3.93)$$

$$\theta(x) = \delta \left( \frac{37}{315} - \frac{2}{315} \hat{\lambda} - \frac{1}{252} \hat{\lambda}^2 \right) \quad (3.94)$$

$$\tau_s(x) = \frac{\mu U_\infty}{\delta} (2 + \hat{\lambda}) \quad (3.95)$$

For the flat plate boundary layer we find from the Momentum-Integral Equation for a quartic velocity profile:

$$\frac{d}{dx}(\delta) = \frac{630}{37} \frac{\nu}{U_\infty} \frac{1}{\delta} \rightarrow \frac{1}{2} \frac{d\delta^2}{dx} = \frac{630}{37} \frac{\nu}{U_\infty} \quad (3.96)$$

Rewriting this equation on the same manner as before gives us the equation for the boundary layer thickness:

$$\delta(x) = \sqrt{\frac{1260}{37}} \sqrt{\frac{\nu x}{U_\infty}} = \frac{5.84x}{(Re_x)^{\frac{1}{2}}} \rightarrow \frac{\delta(x)}{c} = \frac{5.84}{(Re_c)^{\frac{1}{2}}} \left(\frac{x}{c}\right)^{\frac{1}{2}} \quad (3.97)$$

Then with this result for the boundary layer thickness we find the expressions for the displacement thickness, the momentum thickness and the total skin friction coefficient:

$$\delta^*(x) = \frac{3}{10} \delta \quad \rightarrow \quad \frac{\delta^*(x)}{c} = \frac{1.75}{(Re_c)^{\frac{1}{2}}} \left(\frac{x}{c}\right)^{\frac{1}{2}} \quad (3.98)$$

$$\theta(x) = \frac{37}{315} \delta \quad \rightarrow \quad \frac{\theta(x)}{c} = \frac{0.69}{(Re_c)^{\frac{1}{2}}} \left(\frac{x}{c}\right)^{\frac{1}{2}} \quad (3.99)$$

$$C_f = \frac{1}{c} \int_0^c \frac{2\mu U_\infty}{\delta} dx = \frac{1.37}{(Re_c)^{\frac{1}{2}}} \quad (3.100)$$

### 3.3 Numerical solutions [6]

Up to this point we calculated the solutions of the quantities characterising the boundary layer analytically by solving the boundary layer equations using the shooting method or by choosing an approximation for the velocity profile inside the boundary layer. The scope of problems that can be handled by these methods is limited, since this approach is based on a number of assumptions. To expand the possibilities for solving the boundary layer equations, we consider numerical solutions.

#### 3.3.1 Explicit Discretisation

Numerical solutions of the boundary layer equations are based on replacing derivatives by finite-difference approximations. This approximation is called discretisation. We will use this to find numerical solutions for the boundary layer equations. We will start with the boundary layer equations for a steady free stream flow, where we consider again a constant free stream flow:

$$\frac{\partial u}{\partial x} + \frac{\partial v}{\partial y} = 0 \quad (3.100)$$

$$u \frac{\partial u}{\partial x} + v \frac{\partial u}{\partial y} = \nu \frac{\partial^2 u}{\partial y^2} \quad (3.101)$$

The domain containing the boundary layer is divided in small elements: the so-called grid. This grid consists of grid points which are formed by the coordinate lines. This grid is illustrated in figure 3.4. At the grid points we want to determine the unknown velocity components  $u(x, y)$  and  $v(x, y)$ .

We can use this method since we know the x- and y-components of the velocity at a starting line namely the leading edge ( $x = 0$ ) of the horizontal plate. The first step will be to find the new components of the velocity at the grid points on the line  $x = x_{i+1}$ . We will obtain this result by using equation (3.101). Next step is to calculate the vertical velocity at this next grid point.

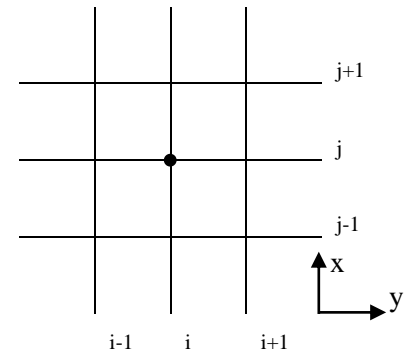


Figure 3.4 Schematic view of grid

Let us examine the difference equations in terms of this grid. We will use the centered space difference expressions to approximate the partial derivative of  $u$  with respect to  $y$ .

$$\left(\frac{\partial u}{\partial y}\right)_{i,j} \approx \frac{u_{i,j+1} - u_{i,j-1}}{2 \cdot \Delta y} \quad (3.102)$$

$$\left(\frac{\partial^2 u}{\partial y^2}\right)_{i,j} \approx \frac{u_{i,j+1} - 2u_{i,j} + u_{i,j-1}}{\Delta y^2} \quad (3.103)$$

We cannot use this method for the partial derivative with respect to  $x$  since the only data available is known for the initial station, and not for a station downstream of this station. Therefore we will use the forward space difference method to approximate the partial derivative with respect to  $x$ :

$$\left(\frac{\partial u}{\partial x}\right)_{i,j} \approx \frac{u_{i+1,j} - u_{i,j}}{\Delta x} \quad (3.104)$$

Now we substitute these three equations in equation (3.101). We obtain:

$$u_{i,j} \frac{u_{i+1,j} - u_{i,j}}{\Delta x} + v_{i,j} \frac{u_{i,j+1} - u_{i,j-1}}{2 \cdot \Delta y} = \nu \frac{u_{i,j+1} - 2u_{i,j} + u_{i,j-1}}{\Delta y^2} \quad (3.105)$$

We can transform this equation to obtain an expression for the x-component of the velocity  $u_{i+1,j}$  at the next station:

$$u_{i+1,j} = u_{i,j} + v \frac{u_{i,j+1} - 2u_{i,j} + u_{i,j-1}}{u_{i,j}} \frac{\Delta x}{\Delta y^2} - \frac{u_{i,j+1} - u_{i,j-1}}{2} \frac{v_{i,j} \Delta x}{u_{i,j} \Delta y} \quad (3.106)$$

Now we have the values  $u_{i+1,j}$  known. With this we can determine the values  $v_{i+1,j}$ . We will use equation (3.100) for this. First, we use a backward difference for  $\partial v / \partial y$  since we know the value of  $v$  one step back in  $j$ , but not one step forward in  $j$ .

$$\left(\frac{\partial v}{\partial y}\right)_{i+1,j} \approx \frac{v_{i+1,j} - v_{i+1,j-1}}{\Delta y}, \quad \text{with } v_{i+1,0} = 0 \quad (3.107)$$

To obtain good accuracy, we can see this as a central difference at a location between grid points  $j$  and  $j - 1$ . We use this fact to approximate  $\partial u / \partial x$  not far from this point at the location between  $i$  and  $i + 1$  and  $j$  and  $j - 1$ :

$$\left(\frac{\partial u}{\partial x}\right)_{i+1,j} \approx \frac{1}{2} \left[ \frac{u_{i+1,j} - u_{i,j}}{\Delta x} + \frac{u_{i+1,j-1} - u_{i,j-1}}{\Delta x} \right] \quad (3.108)$$

Substituting equations (3.107) and (3.108) in equation (3.101) we get:

$$\frac{1}{2} \left[ \frac{u_{i+1,j} - u_{i,j}}{\Delta x} + \frac{u_{i+1,j-1} - u_{i,j-1}}{\Delta x} \right] + \frac{v_{i+1,j} - v_{i+1,j-1}}{\Delta y} = 0 \quad (3.109)$$

Re-arranging this equation leads to the expression for  $v_{i+1,j}$ :

$$v_{i+1,j} = v_{i+1,j-1} - \frac{1}{2} \left[ \frac{u_{i+1,j} - u_{i,j}}{\Delta x} + \frac{u_{i+1,j-1} - u_{i,j-1}}{\Delta x} \right] \Delta y \quad (3.110)$$

### 3.3.2 Step size

We now have the two explicit relations to calculate the x- and y-component of the velocity at the next grid point. The stability of the numerical scheme is an important point to consider. The step sizes  $\Delta x$  and  $\Delta y$  cannot be chosen arbitrarily. The stability criterion for this difference scheme is [2]:

$$\Delta x \leq \frac{1}{2} \frac{u_{i,j} (\Delta y)^2}{\nu} \quad (3.111)$$

We did the calculation for the case for which the maximum  $u_{i,j}$  – the free stream velocity – is 10 m/s and the kinematic viscosity  $\nu$  is  $1.4 \cdot 10^{-5} \text{ m}^2/\text{s}$ . Using this criterion from equation (3.111) we choose  $\Delta x = 0.0005 \text{ m}$  and  $\Delta y = 0.0005 \text{ m}$ . This means that it takes 2000 steps to cover the whole length of the flat plate when its length is 1 m. The extent of the computational domain in y-direction is 0.025 m.

### 3.3.2 Results

In comparison with the analytical and approximation method, we can only obtain results by executing the calculations. First we verify that the method gives the correct results. When we plot the x- and y-component of the velocity at three different x positions, we expect profiles that are independent of the x position, i.e. a similarity solution (Velocity profiles are plotted in terms of the similarity quantities, like we did with the results from the Blasius equations). Here the boundary layer thickness is obtained from the data where  $u = 0.99U_\infty$

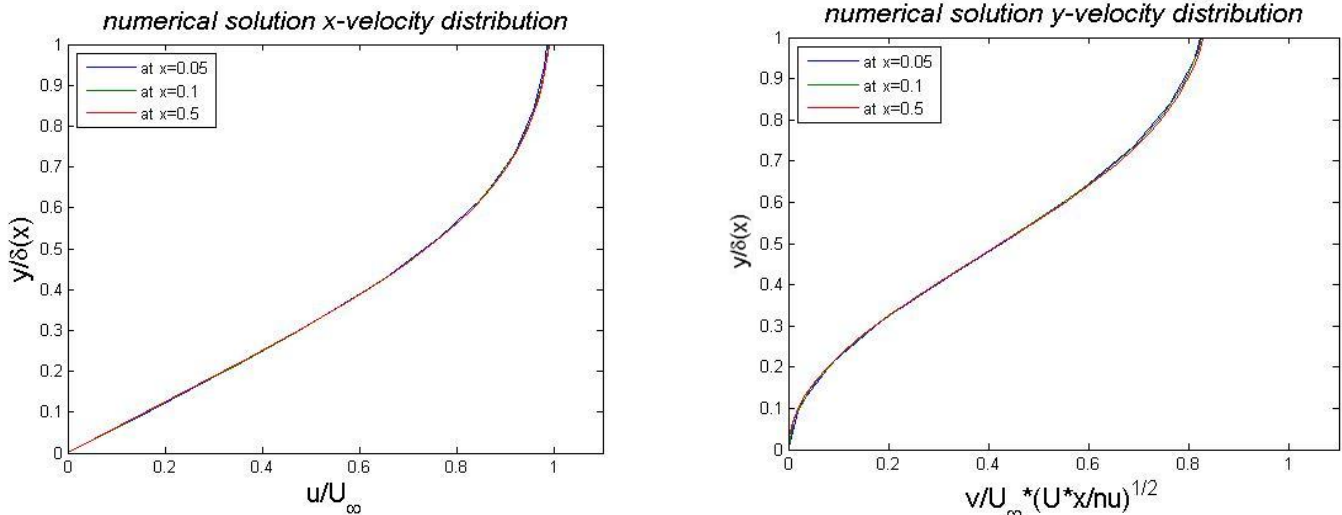


Figure 3.5 x- and y-component of the velocity in the boundary layer as function of  $y/\delta(x)$

We carried out these calculations for a flat plate of 1 m. The results are as expected; the solution is similar, independent of the  $x$  position. The second result we derive from this numerical approach is the skin-friction coefficient. By using a three-point formula using  $u_{i,1} = 0$ , we find the shear stress:

$$\tau_{w,i} = \mu \left( \frac{\partial u}{\partial y} \right)_{y=0} \approx \frac{\mu}{2\Delta y} (4u_{i,2} - u_{i,3}) \quad (3.112)$$

To find the skin-friction drag coefficient, we need to integrate this shear stress following equation (3.39). With the use of the trapezoidal rule we can carry out the integration. We find for the skin-friction drag coefficient:

$$C_f = \frac{1.033}{\sqrt{Re_c}} \quad (3.113)$$

The third parameter we obtain from this numerical approach is the boundary layer thickness. With the definition of the height of the boundary layer at the location where  $u = 0.99 \cdot U_\infty$ , we can find the boundary layer thickness. Since we have found all the values for  $u$ , we only need to look for the coordinates where the horizontal velocity exceeds  $0.99 \cdot U_\infty$ .

### 3.4 Conclusions

We carried out calculations for the flow in the boundary layer and derived the characteristics of the boundary layer using of three different approaches. Let us first summarise the results from the first two methods:

	Blasius Equation	Cubic velocity profile	Quartic velocity profile
definition $\eta$	$\eta = y \sqrt{\frac{U_\infty}{\nu x}}$	$\eta = y/\delta$	$\eta = y/\delta$
velocity profile	$u = U_\infty f'(\eta)$	$u(\eta) = U_\infty \left( \frac{3}{2}\eta - \frac{1}{2}\eta^3 + \lambda(\eta - 2\eta^2 + \eta^3) \right)$	$u(\eta) = U_\infty \left( 2\eta - 2\eta^3 + \eta^4 + \hat{\lambda}(\eta - 3\eta^2 + 3\eta^3 - \eta^4) \right)$
boundary layer thickness	$\frac{\delta(x)}{c} = \frac{4.9}{(Re_c)^{\frac{1}{2}}} \left(\frac{x}{c}\right)^{\frac{1}{2}}$	$\frac{\delta(x)}{c} = \frac{4.64}{(Re_c)^{\frac{1}{2}}} \left(\frac{x}{c}\right)^{\frac{1}{2}}$	$\frac{\delta(x)}{c} = \frac{5.84}{(Re_c)^{\frac{1}{2}}} \left(\frac{x}{c}\right)^{\frac{1}{2}}$
Skin-friction Coefficient	$C_f = \frac{1.328}{(Re_c)^{\frac{1}{2}}}$	$C_f = \frac{1.292}{(Re_c)^{\frac{1}{2}}}$	$C_f = \frac{1.37}{(Re_c)^{\frac{1}{2}}}$
Displacement thickness	$\frac{\delta^*(x)}{c} = \frac{1.727}{(Re_c)^{\frac{1}{2}}} \left(\frac{x}{c}\right)^{\frac{1}{2}}$	$\frac{\delta^*(x)}{c} = \frac{1.74}{(Re_c)^{\frac{1}{2}}} \left(\frac{x}{c}\right)^{\frac{1}{2}}$	$\frac{\delta^*(x)}{c} = \frac{1.75}{(Re_c)^{\frac{1}{2}}} \left(\frac{x}{c}\right)^{\frac{1}{2}}$
Momentum thickness	$\frac{\theta(x)}{c} = \frac{0.664}{(Re_c)^{\frac{1}{2}}} \left(\frac{x}{c}\right)^{\frac{1}{2}}$	$\frac{\theta(x)}{c} = \frac{0.646}{(Re_c)^{\frac{1}{2}}} \left(\frac{x}{c}\right)^{\frac{1}{2}}$	$\frac{\theta(x)}{c} = \frac{0.69}{(Re_c)^{\frac{1}{2}}} \left(\frac{x}{c}\right)^{\frac{1}{2}}$

We note that it appears that the cubic velocity profile is a better approximation for the solution inside the Blasius equation since all the parameters are more accurate than for the quartic profile.

#### 3.4.1 Velocity profile

With the Blasius equation we found an equation for the velocity in the boundary layer depending only on the dimensionless parameter  $\eta_B = \frac{y}{x} Re_x^{1/2}$ . This is not the same parameter which we used for the approximation method  $\eta = y/\delta(x)$ . To compare the four velocity profiles, we will need to do this in the same manner. For Blasius' solution we used:

$$\eta_B = \frac{y}{x} Re_x^{1/2} \quad (3.114)$$

For the approximation method we used:

$$\eta = \frac{y}{\delta(x)} \quad (3.115)$$

The relation between these two expressions is formed by substituting  $\delta(x)$  from Blasius' solution in equation (3.115). This gives:

$$\eta = \frac{y}{4.9x Re_x^{-1/2}} = \frac{1}{4.9} \eta_B \quad (3.116)$$

In the velocity profile of Blasius the edge of the boundary layer lies at  $\eta_B = 4.9$ , with the approximation method lies the edge at  $\eta = 1$ . To compare the solutions we also plot Blasius' solution in terms of  $y/\delta(x)$ .

When we plot these four solutions for the velocity profiles we obtain:

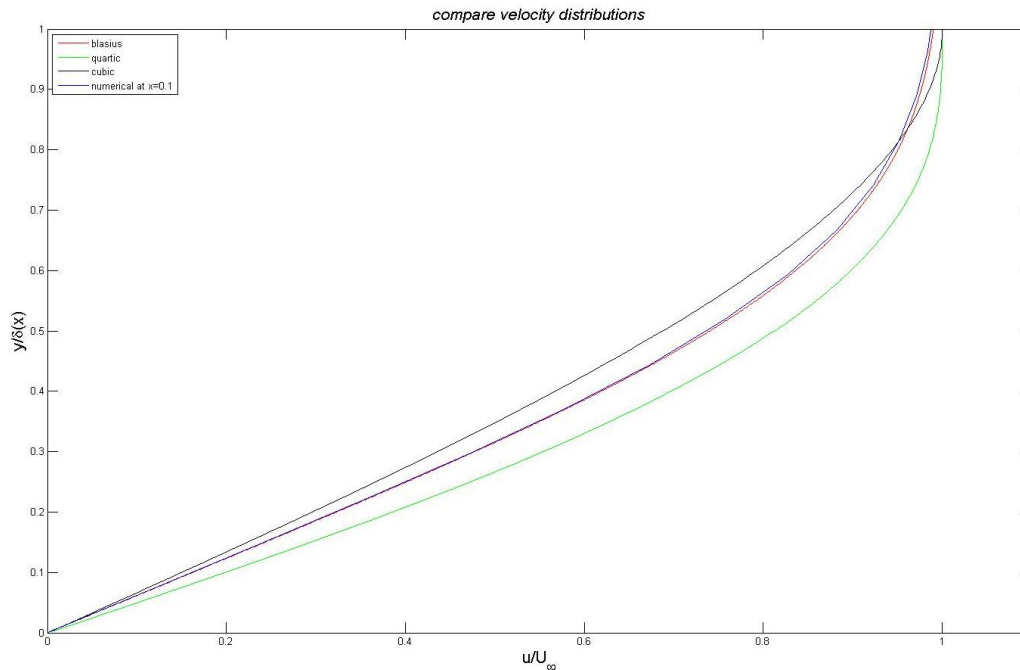


Figure 3.6 Comparison of Blasius' velocity profile with velocity profiles computed using polynomial profiles and numerical method

We observe the failure of the polynomial approximation methods to represent the velocity profile of the Blasius solution. The cubic profile starts with a more accurate slope but fails the curvature near  $\eta = 0$ . The quartic profile starts too slow (or better, it has too high a speed close to the wall), but appears to match the exact solution more accurate near  $\eta = 1$ . The numerical solution shows a very similar velocity profile in comparison with Blasius' solution. This is because in contrast with the approximation methods, the numerical approach has more degrees of freedom. That is the reason that the Blasius and numerical approach are not exactly the same, but agrees quite satisfactorily.

### 3.4.2 Skin friction coefficient

In contrast to the velocity profile, the skin friction drag coefficient of the numerical results is less accurate than the values obtained from the approximation methods based on the Integral Momentum Equation.

Blasius	Cubic	Quartic	Numerical
$C_f = \frac{1.328}{\sqrt{Re_c}}$	$C_f = \frac{1.292}{\sqrt{Re_c}}$	$C_f = \frac{1.370}{\sqrt{Re_c}}$	$C_f = \frac{1.273}{\sqrt{Re_c}}$

The reason of this deviation can be the result of the fact that the numerical method is not accurate near the leading edge of the plate. The first steps of  $\Delta x$  are needed to obtain the correct velocity profile. This can be the cause of the reduced skin friction drag coefficient, since the calculation of the shear stress is not accurate for very small values of  $x$ . In figure 3.7 the local skin friction drag coefficient from the Blasius solution and the numeric solution is plotted as function of  $x$ , where the length of the plate is taken equal to 1. We see the local skin friction drag coefficient from the numerical approach matches the solution from the Blasius solution. However, we observe when zooming in a failure to match the singular behaviour of the Blasius solution that  $c_f(0) \rightarrow \infty$ . The green curve is the local skin friction drag coefficient from the Blasius solution, the red curve that from the numerical approach.

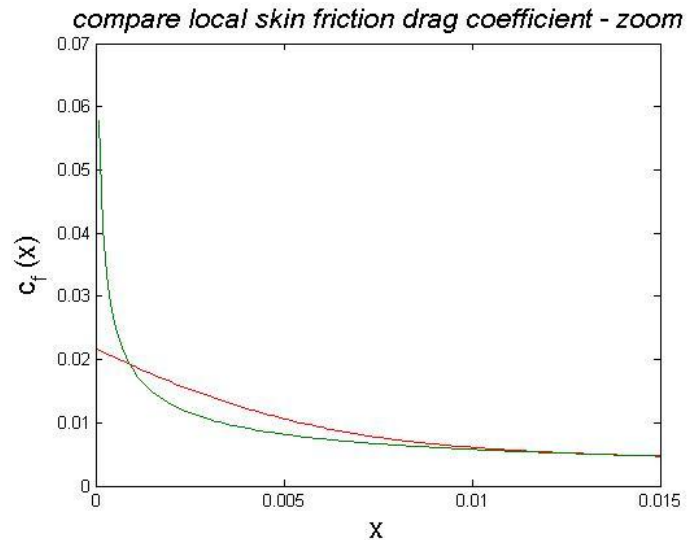
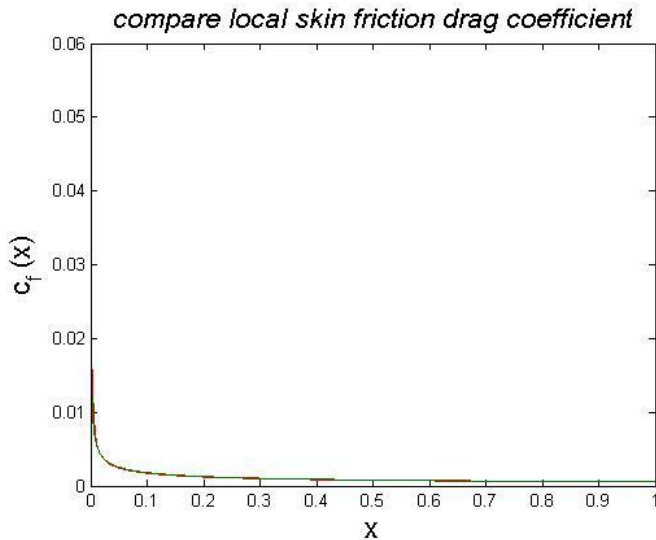


Figure 3.7 Skin friction coefficient as function of x. The green curve is Blasius solution, the red curve the numerical solution

### 3.4.3 Boundary layer Thickness

Also we consider the comparison of the boundary thickness obtained from the different approaches. With each method (analytical, approximation and numerical) we found solutions for the boundary layer thickness. With the use of the quiver function from Matlab, we can obtain a velocity plot for the numerical approach. We only show the velocity vectors for which  $u > 0.99U_\infty$ , see figure 3.8:

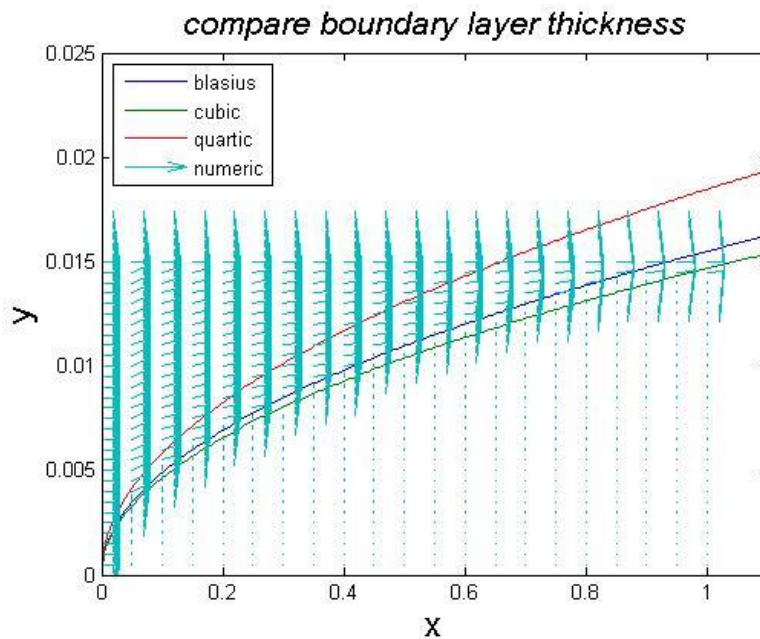


Figure 3.8 Comparison of boundary layer thickness of Blasius' solution with results from the Integral momentum equation and from the numerical solution

To look more closely, we will derive the boundary layer thickness at  $x = 1$ . For this comparison we take  $U_\infty = 1 \text{ m/s}$  and  $\nu = 1 \cdot 10^{-5} \text{ m}^2/\text{s}$ , i.e.  $Re_c = 1 \cdot 10^5$ .

Blasius	Cubic	Quartic	Numerical
$\delta(x) = 0.0155 \text{ m}$	$\delta(x) = 0.0147 \text{ m}$	$\delta(x) = 0.0185 \text{ m}$	$\delta(x) = 0.0141 \text{ m}$

We see that the cubic and numerical method obtain almost the same boundary layer thickness. Both methods are better to predict the boundary layer thickness than the quartic approximation method.

## 4 Experiments

### 4.1 Set-up

Flow velocity measurements are important in many fields. Aeronautics uses it for measuring the speed of a flying object. For weather forecast, environmental departments make use of these types of measurements to carry out research on erosion or irrigation, some authorities need it for measuring at lakes or dams, and so on. In the present experiment it is necessary to measure the velocity of the flow passing over the flat plate to obtain data to compare this with theoretical data from chapter 3.

This experiment is carried out in the silent wind tunnel of the University of Twente. A flat plate - with a specially designed leading edge for the smooth development of the boundary layer – is placed in this wind tunnel at an angle of attack at zero degrees. The flow speed in the boundary layer is measured with the use of Hot Wire Anemometry (HWA). The test set-up is such that the Hot Wire can be varied in height to be able to measure flow speeds in and around the boundary layer. It is possible to vary the height of the Hot Wire with a hundredth of a millimetre (0.00001 m).

#### 4.1.1 Flow speed measurements in boundary layer: Hot Wire Anemometry

Wire probes are used for measurement in air and other gases. HWA is based on the following principle. The probe contains a very thin wire with a voltage difference. Due to this difference a current runs through the wire, resulting in the heating of this wire. When we now place this wire in a flow of air, due to convection the wire cools. HWA will add more energy (voltage) to keep the wire at the same temperature. This increase of energy is a measure for the magnitude of the velocity. When the velocity of the flow is higher, the wire decreases more in temperature, so more energy is needed to compensate this loss in heat.

HWA is capable of measuring velocities from a few  $cm/s$  to velocities of 200 m/s. We will use the miniature wire probe of Dantec which is recommended for 2D-flows. The 1,25 mm long plated tungsten wire has a diameter of 5  $\mu m$ , which results in a short response time.

When we measure with a hot wire, disturbing effects need to be discussed. One of these effects is the temperature dependency of the probe. When there is a varying fluid temperature, it will introduce errors in the measurement. Although the changes will not be that large in this experiment, we use a temperature-compensated probe to minimize the possibility of errors in our measurements[7]. Secondly we discuss the correction needed to measure close to the surface. The probe will lose extra heat due to the presence of the nearby surface. Durst[8] describes in his paper that the correction factor ( $Cu$ ) should be:

$$Cu = U_0/U_{meas} \quad (4.1)$$

With  $U_0$  the actual velocity and  $U_{meas}$  the measured velocity of the flow. The correction factor is needed only close to the body. Durst discusses this ‘close to the body’ with a scaled length  $y^+$ :

$$y^+ = \frac{y}{l_c}, \quad \text{with viscous length } l_c = \frac{\nu}{u_\tau}, \quad \text{with the friction velocity } u_\tau = \sqrt{\frac{\tau_s}{\rho}} \quad (4.2)$$

In experiments Durst notes that if  $y^+$  is larger than 4, there is no need for any correction of the measured velocity. When  $y^+$  is smaller than 4, he gives an equation for the correction factor:

$$\begin{aligned} y^+ > 4 & \rightarrow Cu = 1 \\ y^+ \leq 4 & \rightarrow Cu = 1 - e^{-Ay^+B} \end{aligned} \quad (4.3)$$

With A and B experimentally found coefficients. Durst finds for a wire with aspect ratio of 0.7 and a wire diameter of 5 $\mu m$  values for A and B. In this case  $A = 0.3$  and  $B = 2.2$ . When we substitute these coefficients in the equation for the correction factor we find:

$$y^+ \leq 4 \quad \rightarrow \quad Cu = 1 - e^{-0.3y^{+2.2}} \quad (4.4)$$

#### 4.1.2 Calibration of the Hot Wire

To measure the flow velocity with the Hot Wire, it is necessary to calibrate the probe. For making sure the manner in which calibration is carried out will not affect the measurements, the calibration is carried out in the wind tunnel itself. Also it is necessary to calibrate the probe at the same angle of attack as the angle of attack during the measurements. Bruun [9] describes that the angle of the probe influences the measurement. So the flow needs to come from the same direction as where the flow will come from when the wind tunnel is turned on. Using the funnel shown in the picture in figure 4.1 we are able to blow air in the direction of the probe. This funnel is connected with a device which can measure the pressure in terms of the heights of a water column, a Betz micro manometer. With this we can carefully set the speed of the flow from the funnel and we can calibrate the Hot Wire. Calibration and measurements are executed with the program Streamware Pro V5.02.



Figure 4.1 left: Betz manometer Right: Funnel with probe for calibration

It is also important to calibrate the position of the probe, since the position in the boundary layer influences the velocity. This is carried out with a broken Hot Wire and a multimeter. The multimeter is attached to the surface of the plate (which is of metal) and the ground of the probe. When the broken probe touches the surface, a current will flow which we can measure with the multimeter. Since we suppose that this position is the same for all individual probes, this gives a measure for the position of the probe with respect to the surface of the flat plate. In the discussion of the experiment we will discuss that this method has significant limitations. With this technique we obtain the first data point at a height of 0.15 mm with respect to the surface of the plate.

#### 4.1.3 Flap

The theory describes a flat plate exactly at an angle of attack of zero incidence. In practice the plate is not perfectly flat nor at exactly zero incidence. To find out if incidence is zero, pressure sensors are mounted at the leading edge on both sides of the plate. When the incidence is exactly zero, the pressure will be the same at both sides of the plate. To influence effective angle of attack of the plate, a flap is placed at the trailing edge. When the angle of the flap is adjusted, the stagnation point will move and therefore the pressures on both sides will be different. This is the same mechanism which is used in aircraft wings. With this method we determined that the plate is slightly twisted so that the leading edge is pointing upwards. This can be concluded since the pressure on the lower side of the plate is higher than on the upper side. When the flap is turned  $2.5^\circ$  downwards, the pressures on both sides are equal. This is shown in figure 4.2. Here P1, P2 and P3 are three pressure points at the lower side of the plate with increasing distance from the leading edge. P8, P7 and P9 are pressure points at the same position but on the upper side of the plate. Here we observe that the pressure differences are the lowest when the flap is turned to  $-2.5^\circ$ .

point degrees	P1 (kPa)	P2 (kPa)	P3 (kPa)	P7 (kPa)	P8 (kPa)	P9 (kPa)	difference:	1 - 8 (kPa)	2 - 7 (kPa)	3 - 9 (kPa)
0	-0,0471	-0,0783	-0,1285	-0,0635	-0,0315	-0,1098		-0,0156	-0,0147	-0,0188
-2,5	-0,0393	-0,0661	-0,1080	-0,0615	-0,0320	-0,1063		-0,0073	-0,0046	-0,0017

Figure 4.2 Pressure in kPa on the leading edge of the plate. P1, P2 and P3 are on the lower side, P7,P8 and P9 are on the upper side of the plate

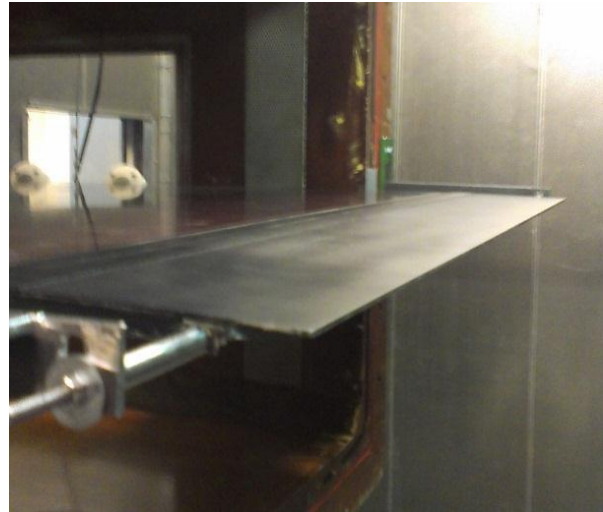
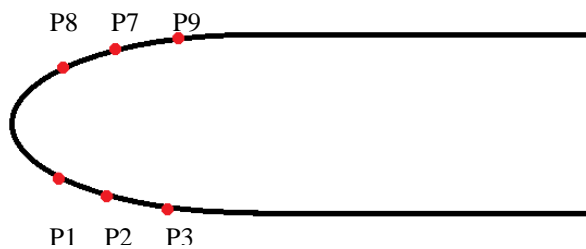


Figure 4.3 Left: Sketch of the positions of the pressure sensors

right: flap at trailing edge of the plate

## 4.2 Results

The conditions at which the experiments have been carried out were the density of air  $\rho = 1.2041 \text{ kg/m}^3$  and a viscosity of air  $\mu = 1.827 \text{ Pas}$ . The free stream velocity is set at 10 m/s and 20 m/s. The measurements were conducted at a distance from the leading edge of  $x = 0.095 \text{ m}$ . With this data we can calculate the local Reynolds number, which indicates whether the flow will be laminar or turbulent. For a free stream velocity of 10 m/s the Reynolds number is  $0.676 \cdot 10^5$  and for 20 m/s the Reynolds number is  $1.357 \cdot 10^5$ , both below the critical Reynolds number of  $5 \cdot 10^5$ . So the flow is expected to be laminar. The height with respect to the surface of the plate is covered in steps of 0.1 mm and starts at 0.15 mm. The data collected from the experiments is presented below.

### 4.2.1 Without flap

The first measurements were executed without the flap since the flap was not ready at the beginning of the experiments. However, this gives us the opportunity to compare the data with and without the flap. The first three experiments were used to acquire experience with the HWA measurements and with the set-up. That is why the data reported begins at experiment 4.

In figure 4.4 the velocity distributions are plotted. The x-axis is the dimensionless velocity where  $u$  is the measured velocity and  $U_\infty$  is the free stream velocity. Along the y-axis the dimensionless height is plotted where  $y$  is the measured height and  $\delta$  is the boundary layer thickness. The boundary layer thickness is found at heights where the measured velocity is not increasing any more. Then we know we reached the edge of the boundary layer. Also with Blasius' solution the boundary layer thickness is calculated and these values confirm the used height for the boundary layer thickness in the experiments.

For the HWA measurements we also need to compensate for the heat lost to the wall. In this case – using the result of Blasius for the shear stress – we only need to correct the values measured at the first data point with a free stream velocity of 10 m/s since we find that  $y^+ = 4$  corresponds to  $y = 1.65 \cdot 10^{-4} \text{ m}$ . For a free stream velocity of 20 m/s we find  $y^+ = 4$  at  $y = 0.98 \cdot 10^{-4} \text{ m}$ , i.e. in the measurement it is not necessary to compensate for the heat lost to the wall.

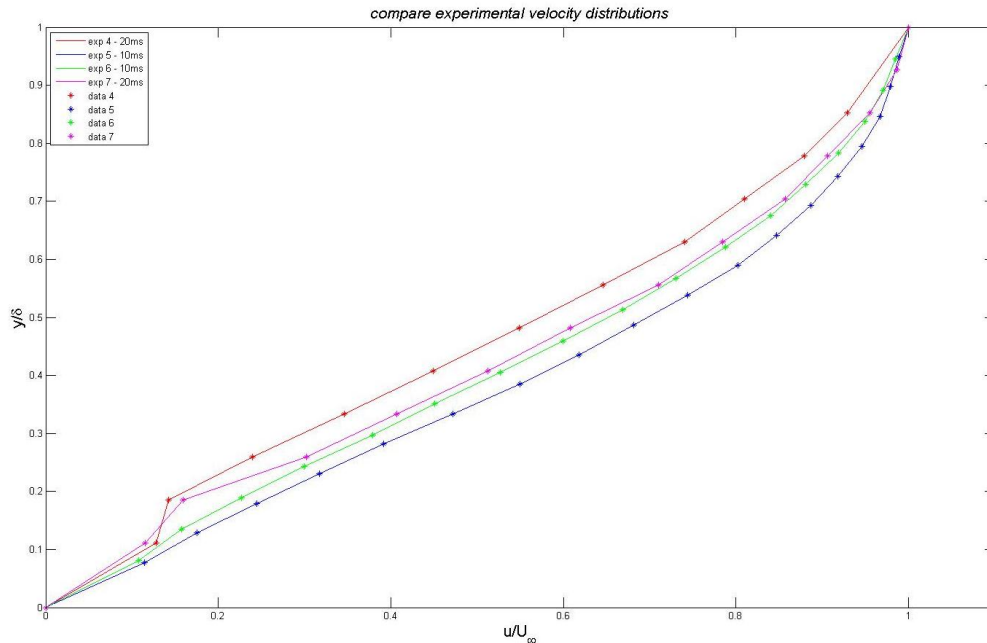


Figure 4.4 Measured velocity distributions at  $x=0.095$  m

We observe some agreements in the results presented in figure 4.3, but they are not exactly the same. This can have a couple of reasons. First, each measurement started with the velocity calibration. This can be a cause for slight variations in the measurements. Second, the measurements for 20 m/s give higher values for the velocity. The reason for this can be the slight deviation of the angle of attack which influences the velocity distribution in the boundary layer more at higher free stream velocities. When measuring the pressures at the leading edge it is observed that the pressure difference increases at higher free stream velocities. Since the pressure at the upper side is lower, the flow on this side of the plate is higher. The flow at the lower side of the plate, where the flow speed is measured in the experiments, is lower. So, a higher free stream velocity causes a higher pressure difference, which leads to lower velocities in the measured boundary layer. Therefore, we observe a lower velocity distribution at free stream velocities at 20 m/s in comparison with the experiments at 10 m/s. Third, a distortion at the second data point is observed for both measurements at 20 m/s which is unexpected. Therefore another measurement is carried out for a free stream velocity of 20 m/s. In this measurement this deviation was not observed, so we conclude that this was a random fluctuation.

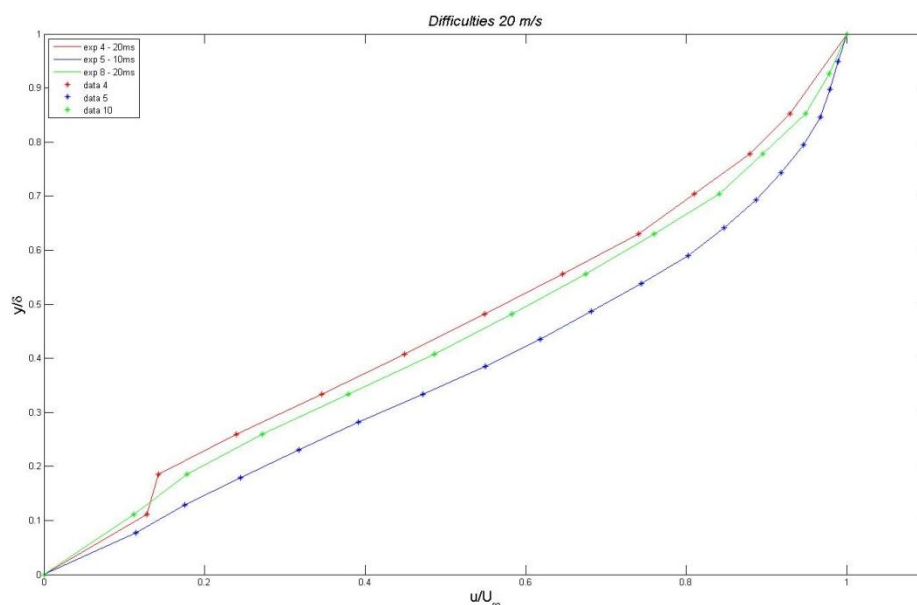


Figure 4.5 comparison experimental velocity distributions with new measurement at 20 m/s at  $x=0.095$  m

### 4.2.2 With Flap

The second measurements has been carried out for the flat plate with the flap attached to the trailing edge. The flap is set at an angle of  $-2.5^\circ$ , in order to have the same pressures on both sides of the leading edge of the plate. Again, free stream velocities of 10 m/s and 20 m/s are used in the experiments. The results are presented in figure 4.6.

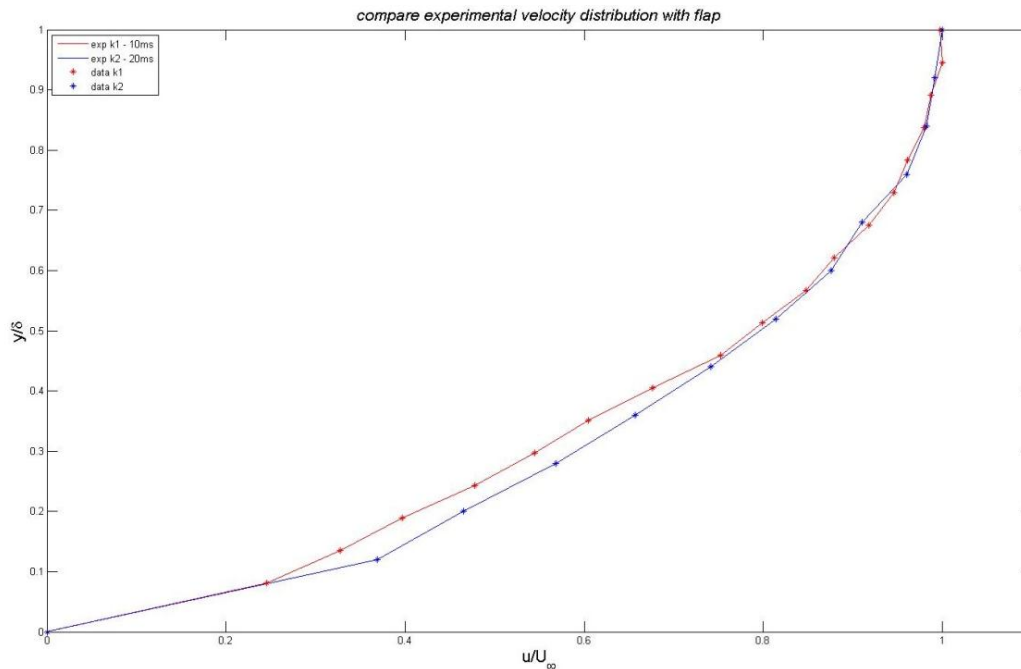


Figure 4.6 Comparison experimental velocity distributions for the flat plate with flap

Here we observe more agreements between the results for the two free stream velocities. Since the flap ensures equal pressures on both sides of the leading edge of the flat plate, the graphs should be similar to each other. Still there are some derivations between both graphs. This can be the cause of failures in the measurements. To find out if the measured dimensionless velocities agree, more experiments should be carried out.

## 4.3 Comparison of data

### 4.3.1 Comparison data with and without flap

Measurements on the pressure on the upper and lower side at the leading edge of the plate show that the plate and/or the oncoming flow is slightly twisted such that the leading edge is turned upwards. When plotting the results from experiments with and without the flap at the trailing edge, we expect for the experiments without the flap a lower velocity distribution, i.e. the curve of the experiments with the flap will shift downwards in the graph. The results are presented in figure 4.7.

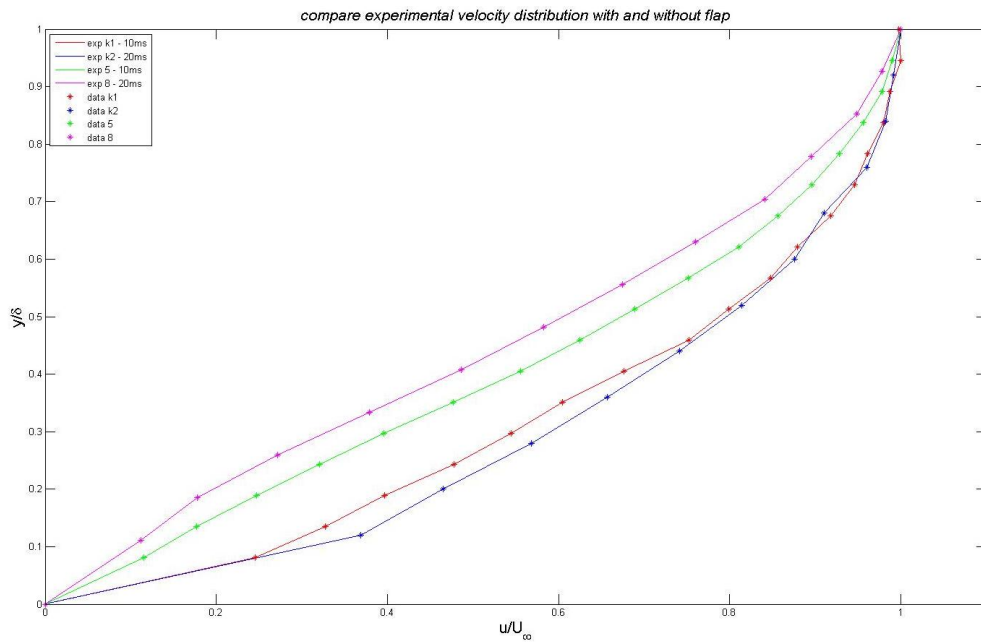


Figure 4.7 Comparison experimental velocity distribution with and without flap

Indeed, the velocity distributions are higher for the experiments with the flap than the experiments without the flap.

### 4.3.2 Comparison experimental data with theory

Now we can compare the data from the experiments with the results from theory described in chapter 3. We only plot the data from the experiments with the flap and we compare this with the Blasius' solution. The results are presented in figure 4.8.

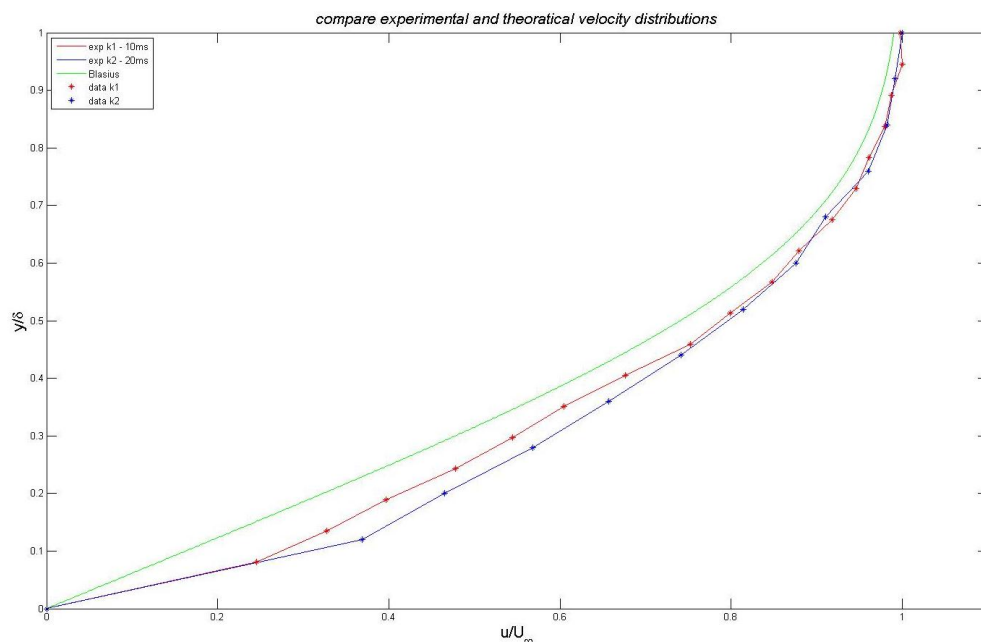


Figure 4.8 Compare experiment with theory

The experimental data indicate higher velocities in the boundary layer than the theory predicts. Nevertheless, the curves appear to follow the Blasius solution quite well. In the discussion the cause of the distortion is explained.

The results can also be presented in another way. We now take the y-axis in a similar way as for the Blasius solution, i.e. as  $\eta_B = \frac{y}{x} Re_x^{1/2}$ . Then we compare the Blasius solution with the data from the experiment with the flap for the free stream velocity of 10 m/s.

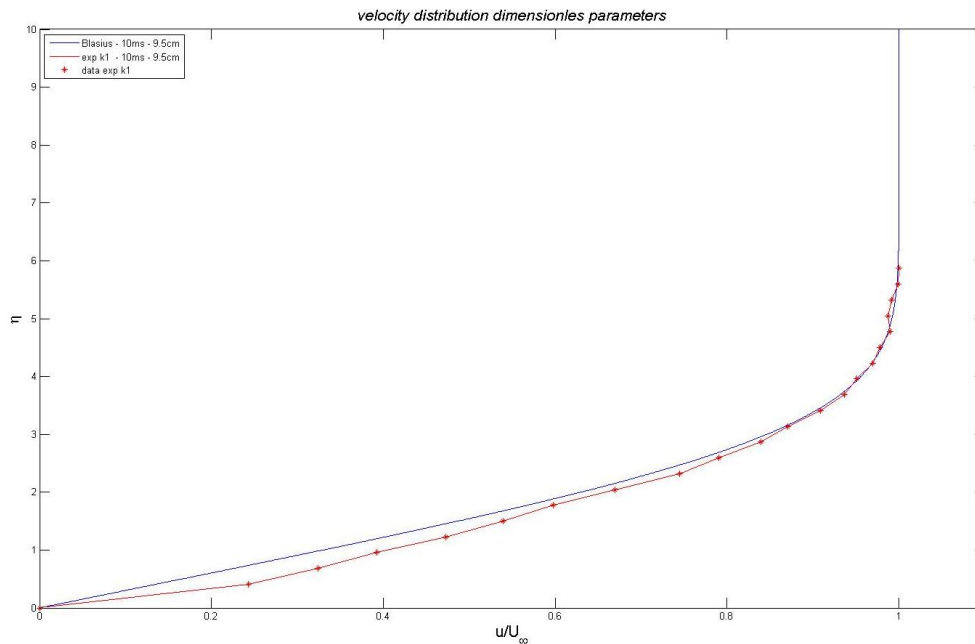


Figure 4.8 Comparison Blasius' velocity profile with the measured data from  $U_\infty = 10$  m/s

This graph confirms the conclusions, that the Hot Wire is capable to measure the velocity in the laminar boundary layer properly. This, because we observe a close similarity between Blasius' solution and the data for a free stream velocity of 10 m/s. Same procedure is done for the measurement for a free stream velocity of 20 m/s. This graph is not put in this report since the figure shows great agreements with figure 4.8 and therefore also confirms the conclusion that the Hot Wire seems to be capable to measure the velocity in the laminar boundary layer properly.

### 4.3 Discussion

Some procedures had certain difficulties which we will discuss here. A major flaw in the experiment is the calibration of the position of the probe.

We used a broken Hot Wire in order to find the location of the probe with respect to the surface of the plate. This is carried out with a broken probe since Hot Wires are fragile and are likely to break when touching the surface of the plate. Here we assume that for every probe and for every measurement the location of the surface of the plate is the same. But since we are working in the very small region of the boundary layer ( $< 2$  mm), differences of tens of millimetres will affect the measurement significantly. Since the data from the experiments with the flap attached to the trailing edge did not match the solution of Blasius, we presume a failure of positioning the Hot Wire. Therefore we measured the location of the surface of the plate with three different broken Hot Wires. Before every measurement the probe was taken out of the probe support. The results are presented in figure 4.9. The probe was turned  $180^\circ$  for measurements 6 to 10.

measurement	1	2	3	4	5	mean	6	7	8	9	10	mean
Probe 1 (mm)	4.34	4.39	4.43	4.41	4.31	4.38	5.29	5.31	5.33	5.28	5.29	5.30
Probe 2 (mm)	4.91	4.98	5.02	4.95	4.92	4.96	5.15	5.18	5.27	5.19	5.21	5.20
Probe 3 (mm)	5.06	5.07	5.10	5.05	5.10	5.08	5.30	5.32	5.28	5.31	5.35	5.31

Figure 4.9 Height measurements with different Hot Wires

These results show differences in the position of the surface of the plate for different probes but also variations within the results for each probe itself. It also shows that the measurement of the height changes when the probe is turned 180°. Where the average height for probe 2 and 3 differ 0.2 mm when turning the Hot Wire, for probe 1 the difference is almost 1 mm. It can be concluded that probe 1 is bent and therefore we cannot use this probe for calibrating the position of the surface of the plate.

So in order to determine the height of the surface we only use probe 2 and 3. Since the heights vary for each probe it is not possible to determine the height within a margin less than 0.1 mm. Therefore the height that is used in the presentation of the results is most likely not accurate. With this knowledge, we can fit the results from the experiments with Blasius' solution. What we mean by this is we set the position of our first measured data point with a certain measured velocity equal to the corresponding height for this velocity from Blasius' solution. With this we can investigate the measurement follow the curve from the Blasius equation. The graph was fitted with the first data point height of 0.23 mm, a difference of 0.08 mm with measured position. The results of fitting the experimental data with the Blasius solution is presented in figure 4.10.

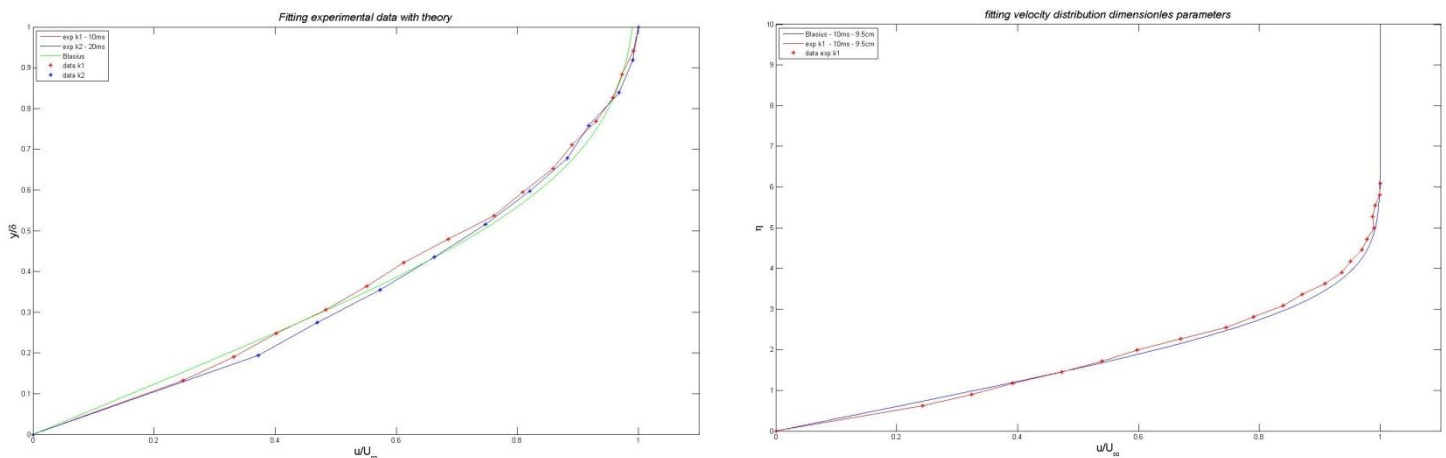


**Figure 4.10** Fitting experimental data with Blasius' solution

This result shows satisfactory agreements with results from Blasius' solution. Three factors can have contributed to this difference in height. First factor can be the unequal lengths of the probes. A slight difference in length of the Hot Wire probes can already contribute substantial to the deviation. Second factor can be the design of the probe holder. The probe is placed in the probe holder like a plug in a socket. The probe can twist slightly in the probe holder. But since we are searching for differences in the range of hundredths of millimetres, this can play a role. Third factor is the wing profile to which the probe holder is attached. This wing can also move slightly. This can also play a role in the deviation of the height of the surface.

Let us secondly discuss the use of the Betz micro manometer. We set the Betz manometer at a particular pressure to obtain a chosen flow velocity. At low speeds ( $< 3$  m/s) the pressure is not varying much, so it is difficult to set the right velocity. Furthermore, it is difficult to read off the pressure precisely. Fluctuations in the use of the Betz manometer give flaws in the calibration of the Hot Wire and therefore in the measurements.

#### 4.4 Conclusions

From these experiments it can be concluded that the Hot Wire data can be fitted with the theory, i.e. Blasius' solution. With the use of the flap the pressure at the upper- and lower side was set at equal values. The set-up for the Hot Wire probe should be reconsidered since we are not able to determine the height of the probe with respect to the surface of the plate accurately. It should be possible to set the height within a margin less than a tenth of a millimetre. Take notion the Hot Wire probe is able to fit to the Blasius solution is a less firm conclusion than when we would be able to find the exact height of the surface of the plate. In this case we can only investigate the potential of following the curve and

we cannot draw conclusions about the actual measuring of the velocity on particular positions. Current set-up is too inaccurate for this.



## 5 Conclusions and Recommendations

### 5.1 Main Conclusions

In the present study analytical, numerical and experimental data has been obtained and analysed concerning the laminar boundary layer over a flat plate at zero degree incidence. In figure 3.6 the comparison between Blasius' solution, the Integral Momentum equation based on von Karman's integral momentum method and the numerical approach is presented. It is clear that the numerical approach produces a velocity distribution that compares very well with Blasius' solution. This numerical approach can be used in situations for which analytical results are not available.

Experiments in the wind tunnel showed that Hot Wire Anemometry measurements are able to fit Blasius' solution. This fitting is presented in figure 4.10. With the use of the flap at the trailing edge, we were able to vary the stagnation point at the leading edge such that the experiments could be compared properly with the theory. Due to the limitations of positioning the probe accurately, we cannot draw the conclusion that the Hot Wire is able to measure the velocity distribution in the boundary layer. However, we can conclude that the results of the measurements with the Hot Wire fit to Blasius' solution and therefore it is expected that in the case of more accurate positioning of the probe, the Hot Wire is able to measure the velocity distribution within the boundary layer.

### 5.2 Recommendations

The most important limitation of this experiment was the positioning of the probe with respect to the surface of the flat plate. On one hand the Hot Wire is very fragile and may not touch the wall, on the other hand the laminar boundary layer was less than 2 mm thick. Since we are working in this thin boundary layer, a difference in position of only a tenth of a millimetre has a significant impact on the results. In section 4.3 we discussed the used method to position the probe and the shortcomings of this method. We will discuss a number of suggestions for improving positioning of the probe.

There are two ways for to position the probe more accurate. First way is to look for a Hot Wire where its lengths are known with small margins of error. In this case, the probe support should be fixed more firmly. With these two conditions, we can calibrate the position of the probe with less margin of error. When these probes are not available, we should find another method to determine the height of the probe with respect to the surface of the plate. Since the probe is so fragile, we should either calibrate the probe contactless or make contact with the surface such that the probe will not break. A specially designed magnetic cube could be mounted to the wall. It should be magnetic to attach it to the wall. This cube has at a specific height a hole of diameter less than 0.1 mm from which air is flowing. With the Hot Wire, we can detect the location of this flow and then the position of the probe is at a certain distance from the wall of the plate. This is positioning the probe contactless. Another option is to develop a probe support with some sort of antenna. The antenna can touch the wall to measure the height of the probe to the wall. The difference between the height of the antenna and the probe itself should then be measured, possibly using lasers.

When the positioning of the probe can be carried out more accurately, it is recommended to carry out more experiments with Hot Wire Anemometry. We can draw conclusions more firmly whether the Hot Wire can indeed be used for measuring the velocity distribution in the boundary layer.



## 6 References

1. Young, A.D., Boundary layers. AIAA education series 1989, Washington, DC: American Institute of Aeronautics and Astronautics : BSP Professional Books. xvii, 269 p.
2. Anderson, J.D., Fundamentals of aerodynamics. 4th ed. McGraw-Hill series in aeronautical and aerospace engineering 2007, Boston: McGraw-Hill Higher Education. xxiv, 1008 p.
3. Çengel, Y.A., Heat & Mass Transfer: A Practical Approach 2007: McGraw-Hill Education (India) Pvt Limited.
4. Schlichting, H. and K. Gersten, Boundary-layer theory. 8th rev. and enl. ed 2000, Berlin ; New York: Springer. xxiii, 799 p.
5. Schobeiri, M., Fluid mechanics for engineers : a graduate textbook 2010, Berlin: Springer. xxi, 504 p.
6. Schetz, J.A., Boundary layer analysis 1993, Englewood Cliffs, N.J.: Prentice Hall. xxii, 586 p.
7. Dynamics, D., Probes for Hot-wire Anemometry, N. Instruments, Editor 2012. p. 25.
8. Durst, F., E.S. Zanoun, and M. Pashtrapanska, In situ calibration of hot wires close to highly heat-conducting walls. Experiments in Fluids, 2001. 31(1): p. 103-110.
9. Bruun, H.H., Hot Wire Anemometry: Principles and Signal Analysis 1995: Oxford University Press on Demand.